Escola de Camins
Escola Tècnica Superior d'Enginyeria de Camins, Canals i Ports
UPC BARCELONATECH

TREBALL FINAL DE MÀSTER

Increased pavement deterioration induced by flooding: A case study of 2013 Colorado floods using stochastic Monte Carlo simulations in discrete-time Markov chains (DTMC)

Treball realitzat per:
Vallès Vallès, David

Dirigit per:
Casas Rius, Joan Ramon - (UPC)
Torres-Machi, Cristina - (CU-Boulder)

Màster en:
Enginyeria de Camins, Canals i Ports

Barcelona, juny 2021

Departament d'Enginyeria de la Construcció

THIS PAGE INTENTIONALLY LEFT BLANK

ACKNOWLEDGEMENTS

A la mare i al pare pel suport, tant moral com econòmic, durant tots aquests anys; encara no tinc clar quin ha estat més gran.

To Professor Cristina Torres-Machi, who accepted me into the Innovation for Resilient Infrastructure (IRI) research group at CU-Boulder. Prof. Torres-Machi provided funds and gave me constant guidance and feedback for the current thesis and the arising journal paper. I can only express gratitude to Prof. Torres-Machi for all these five intense months.

To the College of Engineering & Applied Sciences at the University of Colorado-Boulder, who gave me the chance to join the Europe-Colorado Program, formerly known as Balsells Program, and provided the funding and sponsorship to pursue this research project at CU-Boulder.

To Professor Joan Ramon Casas Rius, who assisted me with my "*Treball de Recerca*" at high school and finally becoming the UPC tutor of this master's thesis. It has been a long but worthwhile journey.

ABSTRACT

ENGLISH VERSION

Road asset managers endeavor to forecast the impact of floods in pavement deterioration, and therefore establishing maintenance operations, budget allocation, or post-flood strategies have yet to be defined in Pavement Management Systems (PMS). Flood events have severely impacted the roadway US network during the last decades, and this trend is forecasted to keep rising due to climate change in most parts of the United States. However, few models assessing the short-term impact of floods were identified, most of them very difficult to implement for network analysis, and no post-flood deterioration trend defined. A comprehensive statistically-based methodology approach determining the conceptual evolution of flooded asphalt sections for the case study from the 2013 Colorado floods is researched and discussed. The results show how the pre-flood road condition influences the loss of pavement condition due to the flood. Once the flood occurs, an important decrease in pavement condition assessing the International Riding Index (IRI) is registered during the first year after the flood for "*Very Good*" and "*Good*" pre-flood conditions, a moderate impact for "*Fair*" pre-flood conditions, and no impact is reported for pre-flood conditions graded "*Poor*" and "*Very Poor*". The long-term pavement deterioration is found to be slightly increased by the flood for "*Fair*" index conditions, and no trend modification is identified for the other cases. The analyses use homogeneous discrete-time Markov chains, calibrated and validated for several Colorado counties. A risk-based approach, using stochastic Monte Carlo simulations and deterministic analyses, is used to quantify the expected loss of pavement condition, using the IRI as a proxy for road deterioration (RD). The case study quantifies the loss in pavement life for flooded pavements, and report that these findings should be considered by road management agencies to optimize its expenditure. Post-flood operational strategies are suggested to minimize the flood impact on asphalt pavements. Finally, the importance of including the flood hazard and their impact on pavement management systems is highlighted.

SPANISH VERSION

Los gestores de redes viarias sufren dificultades a la hora de pronosticar el impacto de las inundaciones en el deterioro del pavimento y, por lo tanto, las operaciones de mantenimiento, asignación presupuestaria o estrategias posteriores a inundaciones aún carecen de integración en los sistemas de gestión de pavimentos. Los eventos de inundaciones han impactado severamente la red de carreteras de EEUU durante las últimas décadas, y se prevé que esta tendencia siga aumentando en la mayor parte de EEUU debido al cambio climático. Sin embargo, se han identificado pocos modelos que evalúen el impacto a corto plazo de las inundaciones, la mayoría de ellos muy difíciles de implementar a nivel de red y no se ha definido una tendencia clara de deterioro posterior a las inundaciones. En la presente tesis, se investigó y discutió un enfoque metodológico integral con base estadística que determina el deterioro de las secciones asfálticas inundadas, para el estudio de caso de las inundaciones de Colorado de 2013. Los resultados muestran cómo la condición de la carretera antes de la inundación influye en deterioro de los pavimentos. Una vez que ocurre la inundación, se registra una disminución importante en la condición del pavimento, evaluada usando el International Roughness Index (IRI), durante el primer año después de la inundación para las condiciones previas a la inundación "*Muy buenas*" y "*Buenas*", un impacto moderado para las condiciones "*Regular*", y no se registra ningún impacto para las secciones que tienen condiciones de IRI "*Deficientes*" y "*Muy Deficientes*". Se encuentra que el deterioro a largo plazo del pavimento aumenta levemente debido a la inundación para condiciones de índice "*Regular*", y no se identifica modificación de tendencia para los otros casos. Los análisis se realizan mediante el uso cadenas de Markov homogéneas de tiempo discreto, calibradas y validadas para varios condados de Colorado. Un análisis de riesgo, aplicando simulaciones estocásticas de Monte Carlo y análisis determinísticos, permite cuantificar la pérdida de condición para pavimentos inundados, utilizando el IRI como índice de deterioro. El caso de estudio cuantifica la pérdida de vida útil del pavimento para pavimentos inundados, y se recomienda que estos hallazgos sean considerados por los gestores de redes viarias. Se sugieren estrategias operativas posteriores a la inundación para minimizar el impacto de la inundación en pavimentos asfálticos. Finalmente, se destaca la importancia de incluir los peligros de inundaciones y sus impactos en los sistemas de gestión de pavimentos.

CATALAN VERSION

Els gestors de xarxes viàries pateixen dificultats a l'hora de pronosticar l'impacte de les inundacions en el deteriorament de paviments i, per tant, les operacions de manteniment, assignació pressupostària o estratègies posteriors a inundacions encara no tenen una clara integració en els sistemes de gestió de paviments. Les inundacions han impactat severament la xarxa de carreteres de EUA durant les últimes dècades, i es preveu que aquesta tendència continuï augmentant en la major part dels EUA causa de el canvi climàtic. No obstant això, s'han identificat pocs models que avaluïn l'impacte a curt termini de les inundacions, la majoria d'ells molt difícils d'implementar a nivell de xarxa i no s'ha definit una tendència clara de deteriorament posterior a les inundacions. En la present tesi, es va investigar i va discutir un enfocament metodològic integral amb base estadística que determina el deteriorament de les seccions d'asfalt inundades, per al cas d'estudi de les inundacions de Colorado de 2013. Els resultats mostren com la condició de la carretera abans de la inundació influeix en deteriorament dels paviments. Un cop que passa la inundació, es registra una disminució important en la condició del paviment, avaluat mitjançant el International Roughness Index (IRI), durant el primer any després de la inundació per a les condicions prèvies a la inundació "*Molt bones*" i "*Bones*", un impacte moderat per les condicions "*Regular*", i no es registra cap impacte per a les seccions que tenen condicions d'IRI "*Deficients*" i "*Molt Deficients*". Es troba que el deteriorament a llarg termini del paviment augmenta lleugerament a causa de la inundació per a condicions "Regular", i no s'identifica modificació de la tendència de deteriorament per als altres casos. Les anàlisis es realitzen mitjançant l'ús de cadenes de Markov homogènies de temps discret, calibrades i validades per diversos comtats de Colorado. Una anàlisi de risc, aplicant simulacions estocàstiques de Monte Carlo i anàlisis deterministes, permet quantificar la pèrdua de condició per a paviments inundats, utilitzant el IRI com a índex de deteriorament. El cas d'estudi quantifica la pèrdua de vida útil del paviment per a seccions inundades, i es suggereix que aquests resultats siguin considerats pels gestors de xarxes viàries. Es suggereixen estratègies operatives posteriors a la inundació per minimitzar l'impacte de la inundació en paviments asfàltics. Finalment, es destaca la importància d'incloure els perills d'inundacions i els seus impactes en els sistemes de gestió de paviments.

TABLE OF CONTENTS

LIST OF TABLES

LIST OF FIGURES

1 INTRODUCTION

In the new global economy, climate change has become a central issue for a wide range of topics, including infrastructure management and the future of the roadway network. Proactive adaptation measures are essential to reduce impact costs of infrastructure adaptation to climate change (Schweikert et al., 2014) and the road network impacts due to climate change are most sensitive to precipitation as well as precipitation and runoff variability amongst different models and policies proposed by (Neumann et al., 2015). For maintaining current levels of services different adaptation measures have been proposed in (Chinowsky et al., 2013) showing the effect of rutting from precipitation will provoke more frequent resealing for paved roads and more frequent re-grading of unpaved roads. The effect of changing levels of precipitation would most affect foundation and pavement design, especially if precipitation levels increase (Meyer et al., 2014). Flooding impacts have a pivotal role in positive consequences, such as aquifer recharge, but inevitably negative consequences like permanent damage in infrastructure assets, varying greatly depending on the location, duration, depth, speed, vulnerability, and value of the environment. Amongst the negative consequences, the deterioration and damage of pavement are found, causing a long-term impact and important economic loss (Geoff, 2011). Approximately, 75% of all Presidential disaster declarations are associated with flooding (US Department of Commerce, n.d.). A primary concern in the US arises from climate models they tend to project increased winter precipitation in the Midwest and Northeast, increasing the risk of early spring flooding as snowpacks melt (Meyer et al., 2014). Even worse when precipitation intensity is projected to increase more, increasing the risk of flooding (Meyer et al., 2014; Tabari, 2020), and hence stationary climate conditions for pavement design can be disrupted (Qiao et al., 2020) under a globally 12% more record-breaking rainfall events registered from 1981 to 2010 (Lehmann et al., 2015).

Road deterioration is a major area of interest within the field of infrastructure asset management. Road deterioration arises in several forms, and from a structural point of view, embankment deterioration and fluvial erosion from intense rain and storms are expected, and a loss of structural foundation on roads from greater seasonal precipitation variation (Vermont Agency of Transportation (VTrans), 2012). Highlighted also by (Meyer et al., 2014) the principal problems to face are greater changes in precipitation levels which derive from the following impacts: roadways closing due to flooding, washouts, and mudslides, or contract in prolonged precipitation, causing pavement heave or cracking. Operations and emergency management and will be more frequent and potentially more extensive emergency evacuations, placing further strain on highways (Meyer et al., 2014).

Road management agencies may require an increase in their budget expenditure to adapt to flooding events (Meyer et al., 2014). Agencies and organizations according to (Wall and Meyer, 2013) share the following concerns "*(1) Data limitations: limited or inaccessible infrastructure data; limited usable climate data. (2) Inadequate treatment of risk: reconciling the immediate need for action with the perception of distant consequences; the qualitative treatment of risk; defining acceptable levels of risk. (3)*

Lack of sufficient financial resources. Transportation agencies and organizations, particularly independent and private-sector organizations, identified additional limitations or barriers: (4) Interdependencies and regulatory barriers. (5) Uncertainty in future system demand; this causes uncertainty in the need for adaptation". Transportation agencies, however, try to offset the beforementioned limitations using risk standards for climate change adaptation and it becomes promising (Wall and Meyer, 2013). Beyond the road agencies, other agencies suffer from these adverse effects such as in municipalities' current income balance and annual result (Unterberger, 2018) or agricultural productivity (Veettil et al., 2021) among others.

A key aspect of sea-level rise and increased hurricane intensity runs into more frequent flooding and damage of coastal roadways (Meyer et al., 2014). An estimated 60,000 miles of coastal highway in the US are already exposed to periodic flooding from coastal storms and high waves (Karl et al., 2009) along with temporary and permanent flooding of roads, erosion of coastal road bases is expected due to rising sea levels and storm surges (Meyer et al., 2014). Most recent flooding models where environmental factors, built with guidance from IPCC RCP curves and the CMIP5 global climate model, are included to understand how flood risk has changed show nearly 11% increase in flood risk over the next 30 years (2050) in (First Street Foundation, 2020). The data in 2020 risks 14.6 million properties (10.3% of all properties) for a 100-year return period (substantial risk implies 1cm of inundation in the properties) and 21.8 million properties (15.4% of all properties) for a 500-year return period. The substantial risk may be highly increased in a property-based analysis following (First Street Foundation, 2020) driving up dramatic changes in most places, ranging from 8% in 2020 to 14% in Jacksonville, FL by 2050 or from 32% to 98% in New Orleans, LA.

Indeed, recovery flood efforts should also consider socio-economic characteristics and vulnerable groups including zones with poor health status and low-income people (Bubeck and Thieken, 2018) where interdependency amongst infrastructure systems and many subsystems were found for developing flood resilient building-roadways networks (Kanti Sen et al., 2021). The characterization of pavement deterioration for flooded sections may enhance to provide these resilient network-based methodologies. There is an urgent need to address the deterioration rates for flooding events and include them in pavement management systems and build resilient infrastructure systems.

2 LITERATURE REVIEW

A literature review was carried out to identify the pavement behavior when flooded, results from different case studies, and finally, current models quantifying the loss of pavement condition and their limitations.

2.1 Flooding impacts on pavement performance

The importance of proactive maintenance policies and the optimal allocation of maintenance resources is fundamental to sustainable pavement design (Torres-Machi et al., 2017) and flood risk management plans provide effective non-structural measures to mitigate flood risk and its consequences (Martinez et al., 2021) but inevitably, climate change forecasts are likely to increase maintenance costs due to several factors such as an increase of temperature that may add additional US$26.3 billion by 2040 (Underwood et al., 2017) to US pavement infrastructure. However, the budget impact of the flood is very difficult to quantify due to its nature and the long-term pavement performance remains unclear.

Extensive research has shown that asphalt concrete (AC) pavements are those suffering the highest deterioration (Gaspard et al., 2007; Helali et al., 2008; Zhang et al., 2008; Sultana et al., 2014; Lu et al., 2018) and limited deterioration was found in Portland Cement Concrete (PCC) (Gaspard et al., 2007; Helali et al., 2008; Zhang et al., 2008). A much-debated question is whether an intermediate deterioration case was found for composite pavements occur as reported by (Gaspard et al., 2007; Helali et al., 2008) but no clear conclusions were reported in (Zhang et al., 2008).

Existing research recognizes the critical role the thickness, and therefore the structural number plays in the flooding deterioration. The thinner the pavements the highest the deterioration after the flood (Gaspard et al., 2007; Helali et al., 2008; Zhang et al., 2008; Khan et al., 2014; Shamsabadi et al., 2014; Sultana et al., 2016c; Hashemi Tari et al., 2015; Texas Department of Transportation, 2019; Asadi et al., 2020). Nonetheless, it was observed pavements with the same structures may carry different load traffics and drainages systems which may highly influence the damage due to flooding (Romanoschi, 2019). One major issue arises in (Wang et al., 2015) noticing the reduction of AC tensile strain is not proportional to the thickness. Strong and high-standard roads amongst AC pavements are suggested by (Khan et al., 2019) to be designed as the best flood-resistance ones, but alarming the environmental costs to offset flooding effects increasing pavement thickness have been highlighted in (Achebe et al., 2021) and sustainable pavement management requires considering environmental aspects at network-level (Torres-Machi et al., 2014).

There is evidence that emergency vehicles carrying high-loading are expected to drive through inundated floods, where the moisture content is extreme, and they play a crucial role exacerbate the damage in an early stage (Sultana et al., 2016c; Lu et al., 2018; Texas Department of Transportation, 2019). The prediction of the structural number helps to determine how much time is needed for the loading capacity to be restored (Mallick et al., 2017) and therefore manage the pavement condition. Strategies

to enhance operations for debris removal might identify the best routes to reduce flood impact over road conditions, creating resilient post-flood strategies.

Previously published studies on the effect of the flood duration over asphalt pavements are not consistent. Controversies arise when they disregard the flood duration as a critical factor (Gaspard et al., 2007; Zhang et al., 2008; Texas Department of Transportation, 2019), whereas in (Lu et al., 2018) because of the MEPDG implementation (*MEPDG*, 2004) it may not be sensitive to short-term extreme precipitations is not clear. In (Wang et al., 2015) the assumption relies on the effect of the flood is time-independent. However, contradictorily models proposed by (Shamsabadi et al., 2014; Hashemi Tari et al., 2015) define the duration and the depth of the flood as an input. Such approaches, however, have failed to address the percentage of subgrade saturation as several authors suggest (Elshaer et al., 2019; Asadi et al., 2020) instead of the depth or duration, which may be used as a proxy for the subgrade saturation but such expositions are unsatisfactory because they fail to address layers permeability where strong correlations are found (Yu-Shan and Shakiba, 2021).

Few studies have investigated pavement age in any systematic way, a report published by (Texas Department of Transportation, 2019) focusing on the flooding impact in Houston showed the older the pavement and found the highest impact on the loss of pavement services which up to 3 years where thin AC layers are placed and also non-linear damage. In comparison, 40 days of reduction is expected according to (Asadi et al., 2020) where no consideration about the pavement age is taken. These conclusions may suggest the influence of pavement age when flooding occurs, however, there has been little discussion addressing the topic.

Other researchers have found that the changes in pavement structural capacity are minimal when the water is below the influencing depth and the base course layer had the highest influence (Elshaer et al., 2019) or analogously the influence of flood gradually diminishes as the water table drops (Wang et al., 2015). Pavement structure and subgrade type significantly impacted the surface deflection, modified structural number and vertical strain, and therefore the rutting performance (Elshaer et al., 2019) if the base layer presents a low-permeability, which leads to longer saturation periods, increase the damage on the pavement (Asadi et al., 2020) and surface deflection and fatigue (Saad, 2014). The time it takes for the subgrade to dry dictates the amount of pavement damage (Texas Department of Transportation, 2019).

Nevertheless, using FWD may show the bearing capacity after flooding but no other distresses which are likely to arise in the following months after the flooding occurs (Romanoschi, 2019) although most previous studies use the FWD and CBW in order to quantify the damage (Gaspard et al., 2007; Helali et al., 2008; Sultana et al., 2016a, 2015; Zhang et al., 2008). Experimental tests carried out in (Wang et al., 2015) show the subgrade stiffness can be recovered after wet-dry cycles even though almost all materials exhibit different patterns between drying and wetting cycles (Nazarian and Yuan, 2012) and the network-level analysis is not easy to perform. Hence, the importance of the post-flood strategies is also highlighted in (Khan et al., 2017a) or alternatively the pre-flood strategies that consider a treatment now to increase

pavement strength for better performance with flooding and a second treatment after a flood (Khan et al., 2016).

Even though some models and methodologies include advanced models for predicting moisture content, they are not able to identify and simulate the real conditions of existing drainages and in-situ distress (Romanoschi, 2019). Additionally, damages regarding stripping of AC layers or potholes can be expected from flooding events (Texas Department of Transportation, 2019) or a rapid localized failure under a heavy load, in the form of a sinkhole (Mallick et al., 2017), D-cracking, freeze-thaw cycles or Alkali-Silica Reaction (ASR) (Romanoschi, 2019).

2.2 Existing models

Models attempting to quantify the flood impact are review in this section. Different approaches and methodologies are reported as well as the data sources and model limitations. A comparison of the existing models for our case study was not possible due to model limitations.

2.2.1 Models according to methodology

Different methodologies can be used in developing predictive models. In this section, a review of the different methodologies used in the researched models is depicted.

Models can be considered probabilistic models such as (Khan et al., 2014) that presented the development of new roughness-based and rutting-based road deterioration (RD) models with flooding. The author proposed probabilistic empirical models with non-homogeneous Markov chains that are much better for RD modeling because of uncertainties in pavement performance, materials, and traffic loading. Further work developed by (Khan et al., 2017b) proposed also gradients such as $\Delta IRI/Pr$, $\Delta IRI/MrL$, and $\Delta Rutting/Pr$ for determining pavement flood resilience following the same methodology but limited data were available to use for validation of the flood risk consequences in (Khan et al., 2017c) where a risk-based methodology was proposed. The risk-based methodology becomes insightful because as different flooding probabilities, different consequences in road performance occur (Khan et al., 2017c) and other models or methodologies which consider a deterministic approach may not tackle this problem conception. Other probabilistic models where the impact of climate change was assessed can be found in (Anyala et al., 2014) where a mechanistic-empirical approach was considered.

On the other hand, the deterministic models exist, which at the same time can be: empirical, mechanistic-empirical or mechanistic models. A regression-based mechanistic-empirical can be found in (Sultana et al., 2016b) where proposes a deterministic model that expresses the structural strength of pavements as a function of time. The model predicts the short-term behavior of a flexible pavement immediately after flooding. Similarly, another model proposed by (Sultana et al., 2016c) presents a mechanistic-empirical deterministic structural deterioration model to predict the rapid deterioration phase of the pavement impacted by river flooding, or the gradual rise of

floodwater. The same author also proposed presents two mechanistic-empirical deterministic-based models for deterioration of rutting and roughness of flood-affected pavements in (Sultana et al., 2018a). A mechanical is addressed by (Saad, 2014) where a coupled finite element analysis was carried out to investigate the effect of the excess water in the granular foundations on the structural performance of flexible pavements. The mechanistic approach of this model makes it no feasible for network analysis but a project one. Note that several authors also remark the empirically or mechanistic-empirical approaches do not capture the stochastic and relevant flooding effects (Wang et al., 2015). Other authors developed deterministic empirical models for flexible pavements in (Hashemi Tari et al., 2015; Shamsabadi et al., 2014) where a stepwise regression was proposed in both models, a mechanistic-empirical natural deterioration developed by (Jackson and Puccinelli, 2006) was adopted to quantify the expected deterioration without considering the flooding event.

Several methodologies and assessments have been proposed by other authors. A methodology used in (Wang et al., 2015) proposed the use of binomial distribution to estimate the numbers and confidence intervals of floods of different severity for pavement analysis and how flood-related damage is sensitive to the severity and frequency of flood. Another framework proposed by (Mallick et al., 2017) consisted of results from unsaturated hydraulic and layered elastic structural analyses. However, the latter is very difficult to apply on network analyses due to the key parameters include soil–water characteristics curve variables, such as suction, moisture content, and hydraulic conductivity, and saturation versus resilient modulus relationship for base course materials. In (Texas Department of Transportation, 2019) researchers translated FEMA flood maps describing the extent of 100-year and 500-year floods into maps estimating local flood water levels/heights using LiDAR data and DEM maps to provide information on the elevation of flexible pavements and used a risk-based methodology to quantify the damage using pavement design software. This method of refining flood probabilities (i.e., flood depth) can be used to investigate flooding scenarios based on an estimate of local floodwater levels (Texas Department of Transportation, 2019) but did not provide a clear model to evaluate but a wide methodology to quantify the damages regarding a given flooding probability.

2.2.2 Models according to location and data sources

In this section, the data sources and the location of the calibrated models are reviewed.

Flooding in Queensland (Australia) from late November 2010 to mid-January 2011 was the main concern for the models proposed by (Sultana et al., 2016b) and (Sultana et al., 2016c). The author studied the affected roads in the Brisbane City Council, the Roads and Maritime Services, New South Wales, and the Department of Transport and Main Roads, Queensland (TMR-QLD). The same events motivated the RD model proposed by (Khan et al., 2014) where the author took 27 road groups using TMR-QLD's 34 000 km road data. The same author in (Sultana et al., 2018a) principally assessed the effects of Cyclone Olga (2010), flooding in January 2011, Cyclone Oswald (2013), and Marcia (2015) in Queensland using data ranging from 2009 to 2015.

The data collected by (Khan et al., 2014) was retrieved from Long-Term Pavement Performance (LTPP) and the National Oceanic and Atmospheric Administration (NOAA). Datasets were collected from January 1996 to December 2013 for the states of Florida, New Jersey, Ohio, and Illinois. Similarly, (Hashemi Tari et al., 2015) used data compiled over twenty years in eight States using the LTPP and NOAA databases as well. It is important to highlight that no particular flooding events were reported in (Shamsabadi et al., 2014) and (Hashemi Tari et al., 2015).

2.2.3 Models according to input requirements

A review of input requirements is the main goal of this section. The formulation of the different models is reviewed to identify the feasibility of its application. In (Sultana et al., 2016c) the modified structural number ratio for the rapid deterioration phase of pavements after flooding was designated as SNC_{rapid} (*Eq 1*).

$$SNC_{rapid} = k_f \cdot \left[1.227 - 0{,}312 \cdot e^{\left(0.011 \cdot t - 0.024 \cdot (CBR + MESA)\right)}\right] \quad \textit{(Eq 1)}$$

The model expresses the SNC_{rapid} as a function of time-lapse in deflection measurement after flooding, subgrade CBR and $MESA$ (*Eq 2*).

$$MESA = 365 \cdot ADT \cdot (\%HV/100) \cdot DF \cdot LDF \cdot N_{HVAG} \cdot (ESA/HVAG) \quad \textit{(Eq 2)}$$

Where ADT is the average number of vehicles per day, $\%HV$ is the percentage of heavy vehicles, DF is the direction factors, LDF is the lane distribution factor, N_{HVAG} is the average number of axle groups per heavy vehicle and $ESA/HVAG$ is the average number of ESA per heavy vehicle axle group. SNC_{rapid} is the ratio of the post-flood SNC_t, at any time t, divided by SNC_i, being i the value pre-flood, $\frac{SNC_t}{SNC_i}$. The SNC values for pavements on granular and cemented bases were calculated using for granular base pavements: $SNC = 3.2{D_0}^{-0.63}$ and for cemented base pavements $SNC = 2.2{D_0}^{-0.63}$. The model was developed with a coefficient of determination (R-squared value) of 0.946, sample size, N was 34 with a 95% confidence interval.

Similarly, in (Sultana et al., 2016b) it proposes the author proposed the SNC_{ratiof} (*Eq 3*) to quantify the damage due to flooding which is only time-dependent.

$$SNC_{ratiof} = 1.032 - 0.034 \cdot e^{\left(\frac{t}{21.5}\right)} \quad \textit{(Eq 3)}$$

Being SNC_{ratiof} the ratio of the modified structural number of pavements after time t of flooding to the modified structural number before flooding $SNC_{ratiof} = SNC_t / SNC_{preflood}$. The SNC values for pavements on granular and cemented bases were calculated using for granular base pavements: $SNC = 3.2{D_0}^{-0.63}$. The model was developed with a coefficient of determination of 0.785 when sample size N was 34 with a 95% confidence interval. The same author proposes a rutting-based (*Eq 4*) and

roughness-based (*Eq 5*) proposed in (Sultana et al., 2018a) expressing the deterioration as a function of time-lapse.

$$\Delta Rut_{post-flood} = k_{rut} \cdot \left[0.083 \cdot t \;\; 0.85 + 0.109 \cdot Rut_{pre-flood} - 0.746\right] \quad \textit{(Eq 4)}$$

$$\Delta IRI_{post-flood} = k_{rg} \cdot \left[0.039 + 0.027 \cdot \sqrt{t}\right] \quad \textit{(Eq 5)}$$

The rutting model was developed with a coefficient of determination of 0.67, a 95% confidence interval, and sample size, N was 436. The total road sections were 218 and each road section contributed two data points. The regression coefficients of the independent variables were fitted by minimizing the least standard error. The roughness model was developed with a coefficient of determination of 0.319, sample size, N, was 436 with a 95% confidence interval. The total road sections were 218, and each road section contributed two data points. The regression coefficients of the independent variables were fitted by minimizing the least standard error.

The model proposed by (Shamsabadi et al., 2014) considers both a natural deterioration model and the increase of IRI due to flooding. The natural deterioration model (*Eq 6*) is proposed by (Jackson and Puccinelli, 2006).

$$\ln(\Delta IRI + 1) = A\left(4.5FI + 1.78CI + 1.09FTC + 2.4P + \frac{5.39\log(ESAL)}{SN}\right) \quad \textit{(Eq 6)}$$

Where ΔIRI is the change in International Roughness Index, A the pavement age, FI the freezing index, CI the cooling index, FTC the freeze-thaw cycles, P the precipitation, $ESAL$ the Equivalent Single Axle Load, and SN the structural number. Eight parameters were entered into a stepwise regression model for 28 sections affected by a single flood, the remaining 7 sections were used for testing, and the proposed equation (*Eq 7*) for determining the change in the IRI due to the flooding.

$$\%\Delta IRI = 10.7 - 1.66NIRI + 7.30NDep - 2.10NDurat + 14.3Dep * IRI \quad \textit{(Eq 7)}$$

Where $\%\Delta IRI$ is the percentage increase due to the flood, $NIRI$ the normalized IRI of the section before the flood, $NDep$ the normalized depth of the flood, $NDurat$ the normalized duration of the flood, the Dep and IRI are no longer described in the model. Similarly, the model proposed by (Hashemi Tari et al., 2015) uses the same natural deterioration model proposed by (Jackson and Puccinelli, 2006). A stepwise regression was implemented separately on two sets of the acquired data: sections impact by floods, sections impacted by snowstorms. It used 28 sections affected by a single flood and 7 sections used for testing which led to a 93% correlation. The increase due to the flood event is expressed by means of a change in the IRI (*Eq 8*). The deterioration considering the flood is calculated according to (*Eq 9*).

$$\%\Delta IRI_F = -4.47 - 0.48IRI + 0.23NDep - 0.57Durat - 26.49NS - 0.49Dep * IRI \quad \textit{(Eq 8)}$$

$$\Delta IRI = \Delta IRI_N + \Delta IRI_F + \Delta IRI_S \quad \textit{(Eq 9)}$$

Where ΔIRI_N is the increase in IRI due to natural causes (*Eq 6*), which used the same as (Shamsabadi et al., 2014), the ΔIRI_F the increase in IRI due to a single flood using (*Eq 8*) and ΔIRI_S the increase in IRI due to a single snowstorm, which is not considered relevant in this study.

Both authors (Hashemi Tari et al., 2015) and (Shamsabadi et al., 2014) do not clearly specify the variables and how they are retrieved nor the differences between the normalized variables and the "non-normalized". Furthermore, no information regarding the units can be found in (Hashemi Tari et al., 2015) and (Shamsabadi et al., 2014). Lessons learned about the relationships between topography, roads, and flooding are highlighted in (Texas Department of Transportation, 2019) but totally disregarded in (Hashemi Tari et al., 2015) and (Shamsabadi et al., 2014). Hence, these two models will be disregarded for the current study as far as no trustable information from them can be retrieved.

Finally, the probabilistic model proposed by (Khan et al., 2014) roughness and rutting versus time are assessed to obtain trends on pavement performance for a road group, and with and without flooding transition probability matrices are generated from the change in trends. These matrices are used applying the Monte Carlo method simulation to obtain roughness and rutting-based road deterioration models for a road group. random variables are generated to select either with or without flood transition probability matrices. Then, another set of random variables is used to compare with the condition states. After 10,000 trials for a 20-year period, the average road deterioration model is obtained.

2.2.4 Model limitations

All models reviewed include several limitations. In this section, model limitations are set and identified as crucial to avoid the applicability of the models.

The limitations on the model proposed by (Sultana et al., 2016b) are 1) the model is only applicable to lightly trafficked local roads with thin asphalt surfacing 2) the ratio of the modified structural strength of the pavement post-flood to modified structural strength pre-flood SNC_{ratio} must be greater than 0.75 and less than or equal to 1; 3) the post-flood reduction in deflection should be 25–40%; and 4) the time is less than 42 days i.e., 6 weeks (t < 42 days) because the original dataset was collected within this time limit.

Limitations in (Sultana et al., 2016c) are highlighted as 1) Applicability to local roads with an asphalt layer thickness of 45–60 mm and gravel layer of 135–200 mm, traffic loading less than 10^5(MESA < 0.1) and over 20 years is the design life period considered in the model. 2) Data with an increase in the post-flood deflection from 25% to 40% was used for the model. 3) The ratio of SNC of the pavement post-flood to SNC of the pavement pre-flood must be greater than 0.75 and less than or equal to 1. 4) Data with a decrease in the post-flood subgrade CBR of more than 30% was used for the model. 5) Post-flood strength was predicted within the time limit of 42 days; that is, within 6 weeks of

flooding, as the original dataset was collected within this time limit. 7) The design traffic loading, MESA, is a constant for this model.

The same author in (Sultana et al., 2018a) proposed the following boundaries and considerations 1) Sections that had pre- and post-flood rutting and roughness data, with post-flood values greater than pre-flood values, were selected to quantify the rapid deterioration phase after the flooding event. 2) Sections with at least 5% loss of surface condition (rutting and roughness).

The models reviewed cannot be either applied and verified to other floods and locations. They generally request difficult input requirements and they are very restrictive regarding the temporal boundaries. Furthermore, the nature of the mid to long-term pavement performance for flooded pavements remains unclear. Very little is currently known about the deterioration process for flooded pavements and if the deterioration depends on the pre-flood condition and how the deterioration process differs from a non-flooded pavement. To address this gap in the literature the central thesis of this study gives answers to these uncertainties. A methodology is developed to address and giving an answer to these questions.

3 METHODOLOGY

The deterioration of pavements due to flooding has been largely analyzed in the literature review (Gaspard et al., 2007; Helali et al., 2008; Sultana et al., 2018b) using either single measurements or measurements collected within a short period of time after flooding. Nevertheless, the impact of flooding on the subsequent performance of pavements has not been studied in depth. The main goal of this research is to cover this gap and characterizes the performance of flooded pavement in the first 5 years after the flood event. The research is aimed at answering four research questions:

1. Does the flood impact the pavement deterioration?
2. How should we conceptually model the deterioration trend induced by the flooding?
3. How much differ this flooded deterioration trend from the non-flooded trend?
4. How much the loss of life expected from the flooded sections differ compared to the non-flooded ones?

To answer these questions, this research analyzes the floods occurring in Colorado, United States, in September 2013. During September 9 and 15th, 2013 a heavy rainfall exceeding 450 mm, combined with a multistate flood flowing tributary waters down, caused destruction which had not been witnessed in Colorado for decades, impacting most of Boulder and Larimer counties (Gochis et al., 2015).

The scope of the analysis covers the pavement deterioration in the most affected counties, as well as counties barely affected by the event. The former will be used to characterize flooded pavements, while the latter will be used as a benchmark of non-flooded pavements. Considering these criteria, the analysis considered the counties of Adams, Arapahoe, Boulder, Jefferson, Larimer, and Weld (*Figure 1*). The criteria set to define the analysis boundaries pointed to the need to reduce the stationary climate uncertainties and the Colorado Front Range counties have been selected. The counties included in the analyses contain presumably the highly-impacted flooded road sections in counties such as Boulder and Larimer, and counties where the flood and precipitation were negligible such as Weld. A major advantage of this approach is to determine extreme cases, where the flood highly impact and where was negligible, for similar environmental conditions.

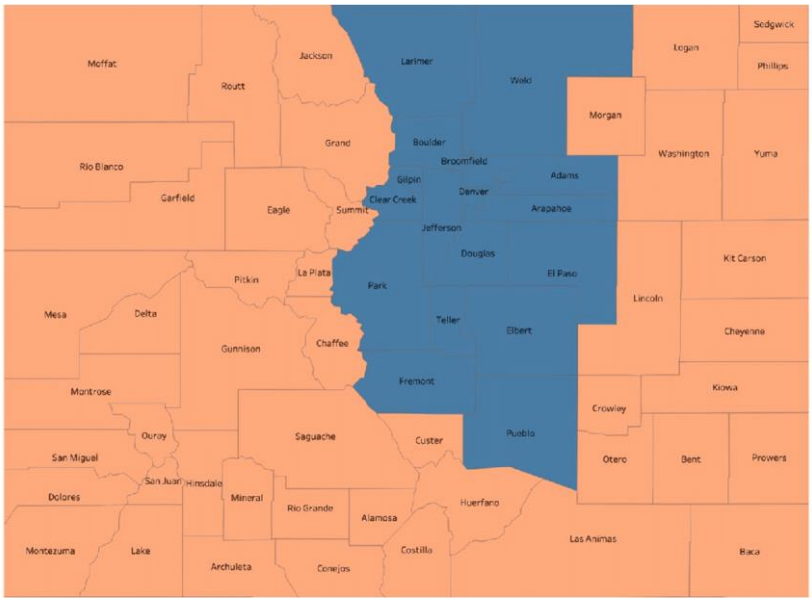

Figure 1: Colorado counties. In blue Colorado's Front Range counties. Source: (Chriestenson and Thilmany, 2020)

3.1 Identification of flooded and non-flooded pavements

The first step in the process was to identify flooded and non-flooded road sections. Due to a lack of flooding maps or identifiers to delimit sections affected by the flooding, a standardized process was developed to determine which pavements in the network were flooded and which were not. The process consisted in identifying the flooded zones as these zones posed on a "*Very High Risk*" (VHR) flooding zones with "*Heavy precipitation*" (HP) registered during the storm, and analogously, the "*No Risk*" (NR) flooding zones with "*No/few Precipitation*" (NP) were considered as non-flooded sections. An overall of 9 combinations arose from 3 flooding risks and 3 precipitation levels identified (*Table 1*). The intermediate cases were disregarded and no longer considered due to the uncertainty they may carry.

		Flooding Risk Zone		
		No Risk	**Moderate-High Risk**	**Very High Risk**
Precipitation registered	**No/Few Precipitation**	**NP-NR**	NP-MHR	NP-VHR
	Moderate Precipitation	MP-NR	MP-MHR	MP-VHR
	Heavy Precipitation	HP-NR	HP-MHR	**HP-VHR**

Table 1: Flood hazard risk and precipitation matrix

The highway system under analysis consisted of public highways managed by the Colorado Department of Transportation (CDOT), including interstates, US highways, and state highways. The geographic and spatial data of this network was obtained from CDOT's Online Transportation Information System ("CDOT Online Transportation Information System," 2021). The shapefiles (*.shp*) were analyzed using an open-source geographic information system (GIS) application called QGIS 3.16 ("QGIS," 2021). The

pavement condition dataset was retrieved from the data collected by CDOT as part of their annual condition assessment, whose supervision is under the Federal Highway Administration (FHWA). Due to the lack of data regarding pavement structure and thickness, which may influence the deterioration process, the functional class was used as a proxy for the pavement thickness and the annual average daily traffic (AADT).

To determine whether the flood affected or not a given pavement section, the analysis considered a combination of risk flooding maps from the Federal Emergency Management Agency (FEMA) ("National Flood Hazard Layer (NFHL) Status," 2021) and the storm precipitation from the Weather and Climate Toolkit (WCT) developed by the National Oceanic and Atmospheric Administration (NOAA) ("NOAA's Weather and Climate Toolkit," 2021).

Risk flooding maps from FEMA's National Flood Hazard Layer (NFHL) were used to identify the following four zones: "*1. Area of Minimal Flood Hazard*", considered a "*No Risk*" zone in the study, "*2. Area of 0.2 PCT Annual change*" considered a "*Moderate Risk*" zone, "*3. Area of 1 PCT in Future Conditions*" considered a "*High Risk*" zone, and "*4. Floodway*", which is considered a "*Very High Risk*" zone. The polygon files defining these flood risk zones were intersected with the highways georeferenced file. "*Moderate Risk*" and "*High Risk*" zones were merged in a single group.

The intensity of the heavy rain event was evaluated using the Digital Storm Total Precipitation map from the 160 high-resolution Doppler weather radars NEXRAD-Level-III from NOAA's Weather and Climatic Toolkit ("NOAA's Weather and Climate Toolkit," 2021). This evaluation was performed from the map captured on Friday 13th September 2013 at 15:08:00. to obtain. This date was deemed representative of the flood event because the peak precipitation period occurred between September 11th and 12th (Hamill, 2014), and the flood duration took days to weeks (Gochis et al., 2015). The accumulated precipitation intensity was divided in three raining intensities: (1) "*No/few precipitation*" if the precipitation intensity was less than 2 inches; (2) "*Moderate precipitation*" for intensities between 2 and 5 inches; and (3) "*Heavy precipitation*" for intensities larger than 5 inches. The raster map containing the accumulated precipitation was vectorized and intersected with the combined highways and the flood hazard zone layers.

Sections experiencing "*1. No/few precipitation*" and located on "*1. Area of Minimal Flood Hazard*" are considered that sections did not suffer the flood. Contrarily, the sections experiencing "*3. Heavy rain*" and georeferenced over "*4. Floodway*" zones are considered the sections the flooding impacted them heavily.

3.2 Development and validation of pavement deterioration models for flooded and non-flooded models

In this research, the pavement deterioration process was modeled as a Markov stochastic process. Markov chains have been widely used in a large number of applications such as physics, biology, operational research, economics, communication networks, among others (Sericola, 2013). Markov models have been also extensively

used to predict pavement deterioration (Butt et al., 1987; Pulugurta et al., 2013; Thomas and Sobanjo, 2013). To incorporate the uncertainties in this deterioration, stochastic Monte Carlo simulations were used (Khan et al., 2017c; Osorio-Lird et al., 2017) and equally length states are performed as suggested by (Butt et al., 1987). The good performance of using Markov chains to assess pavement deterioration under flooded and non-flooded conditions was already reported (Khan et al., 2014).

Markov chains reported in (Yamany et al., 2021) for characterizing pavement deterioration are homogeneous Markov chains, staged-homogeneous Markov chains, semi-Markov techniques, and non-homogeneous Markov chains. Having 5 yearly deterioration measures, the homogeneous Markov chains were found to be the most suitable for the research.

The deterioration index chosen to assess the road deterioration was the average International Roughness Index (IRI). IRI was deemed appropriate because it is often used as a metric of pavement deterioration (Al-Omari and Darter, 1995) and was found to be a good proxy to predict the mean Pavement Serviceability Rating (PSR) (Gulen et al., 1994). Moreover, models proposed by (Shamsabadi et al., 2014; Hashemi Tari et al., 2015; Sultana et al., 2018b) also used the IRI for assessing the flooding impact. The use of Monte Carlo simulations minimizes the pavement age problem, which is a crucial variable for IRI evolution (Pérez-Acebo et al., 2020), but homogeneous Markov chains cannot deal with the pavement age as a variable (Yamany et al., 2021). Performing analysis simulating the deterioration process from the best to the worst condition evolution employing stochastic probabilities was found the best solution to minimize the lack of pavement age.

Two different deterioration models were developed using transition probability matrices for discrete-time homogeneous Markov chains, such that the Markov chain $X(t)$ fulfills $P(X_n = s|X_0 = x_0, X_1 = x_1, \dots, X_m = x_m) = P(X_n = s|X_m = x_m),\ \forall\ 0 \leq m < n$. This assessment is based on the assumption future conditions depends only on the current condition, and the transition matrix at any time n satisfies $(i)\ p_{ij}(n) \geq 0, \forall i, j$ and $(ii)\ \sum_j p_{ij}(n) = 1, \forall i$ (*Figure 2*). This probabilistic modeling combined with stochastic Monte Carlo simulations allows to capture the associate randomness pavement condition evolution (Osorio-Lird et al., 2017) and a deterministic approach assuming the pavement deterioration evolves according to the transition probability matrix (Yang et al., 2005). The matrices essentially contain the probabilities a section has to change the state condition from one year to the following one.

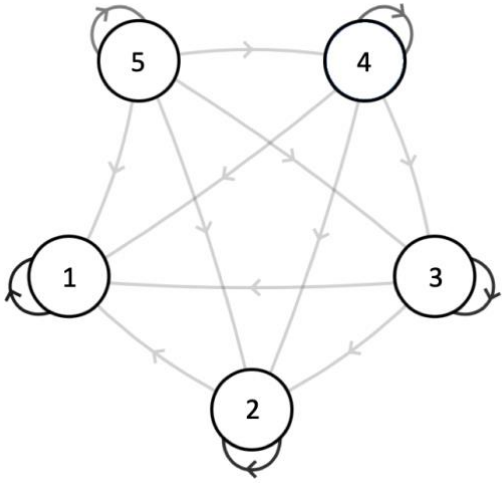

Figure 2: Homogeneous Markov chains for pavement deterioration. Condition decreases from State 5 "Very Good" to State 1 "Very Poor"

The first Markov model was calibrated using the flooded sections and the second model was calibrated using the non-flooded sections. Using this approach, the deterioration forecast for the flooded and non-flooded sections was assessed. The method was able to perform simulations of the flooded sections as if they never suffered the effects of the flood event and therefore, the flood effect was quantified.

The dataset of pavement conditions used to characterize pavement deterioration contained a pre-flood measurement (i.e., taken in 2013 before the flood event) and 5 post-flood measurements (i.e., taken annually between 2014 and 2018). Pavement condition is measured every 0.1 miles.

Maintenance operations and anomalies collecting the data were included in the deterioration dataset. These data points were disregarded and transition probability matrices with states never upgraded were developed. These maintenances and anomalies would have provided transition probabilities where the states could have improved and provide inconsistent analyses. The *Bid Analysis and Management System* (BAMS) dataset from *CDOT* contained the maintenance performed in the different sections throughout the years. The rehabilitations found in the BAMS dataset from 2013 onwards are listed as follows.

1. AMDO (Asphalt Medium Overlay) – Standard HMA mix. Typically, 2 to less than 4 inches thick.
2. AMFL (Asphalt Mill & Fill) – The existing asphalt is milled (typically up to 2" deep, but may vary based on the project), and the milling are removed. Then an overlay is placed over the milled surface.
3. AMJO (Asphalt Major Overlay) – Standard HMA mix. Typically, 4 to less than 6 inches thick.
4. AREC (Asphalt Reconstruction) – Asphalt reconstruction. 5. ASMA (Stone Mastic Asphalt) – A gap graded mix having essentially no voids and requiring more asphalt in the mix. Normally placed on the top surface of a pavement structure and acts as a wearing course. May also include milling of the existing surface.

The *BAMS* dataset containing registered maintenance was used to determine which sections were rehabilitated and the deterioration measurements excluded since the rehabilitation was carried out. Similarly, to identify unregistered maintenance in the dataset, the criteria for the identification for a given section was that $\forall i$ where $i = 2013,2014,\dots,2016$ if $IRI(i) + tol > IRI(i+1)$ and $IRI(i) + tol > IRI(i+2)$ occurring simultaneously, sections from $i+1$ to 2018 were removed. Anomalies collecting the data were expected and a criterion to remove them was set according to $IRI(i) + tol > IRI(i+1)$ and $IRI(i+2) + tol > IRI(i)$, being $IRI(i+1)$ the anomaly. Once all the filters were done, the sections remaining with only one observation were cleared. Extreme values of IRI (i.e., above the 90th percentile) were removed from the analysis due to the loss of a sense analyzing IRI extreme values.

A ride index ($RIDX$) ranging from 100 to 0 was used to develop the Markovian models from IRI (*Eq 10*). This index was used because CDOT classifies its pavement condition in using this standardized index (Keleman et al., 2008), and at the same time, this standardization allowed to easily segregate the deterioration in different states, clearly indicating $RIDX = 100$ indicates a perfect pavement condition and $RIDX = 0$ a very poor pavement condition. This ride index also allowed to helpfully define the groups in the transition probability matrices qualitatively and providing a comprehensive understanding of the state condition regardless of the number of groups and IRI values.

$$RIDX = 100 - \frac{IRI - \min(IRI)}{\max(IRI) - \min(IRI)} \qquad \textit{(Eq 10)}$$

The accuracy of the Markovian models was assessed by means of the root mean square error (RMSE) (*Eq 11*).

$$RMSE = \sqrt{\frac{1}{N}\sum_{i}^{N}\left(RIDX_{i,predicted} - RIDX_{i,measured}\right)^2} \qquad \textit{(Eq 11)}$$

Several matrix sizes were explored, proposed, and analyzed to determine the Markov model providing the best results. The 80% of data from each family was used to calibrate the transition probability matrix and the remaining 20% is used to validate the model.

For the non-flooded transition probability matrix validation, a non-parametric Wilcoxon signed-ranked test was performed to compare the mean differences between paired samples at the 5% significance level H_0: $\mu_{RIDX,Predicted} = \mu_{RIDX,Measured}$. This test was found appropriate because the differences between the $RIDX_{i,measured}$ and $RIDX_{i,predicted}$ were not normally distributed when performing a non-parametric one-sample Kolmogorov-Smirnov test, testing the null hypothesis that the data obtained from the difference comes from a standard normal distribution with unknown standard deviation at the 5% significance level H_0: $\mu_{RIDX,Predicted} - \mu_{RIDX,Measured} = 0$. The data for the one-sample Kolmogorov-Smirnov test was normalized such that $\tilde{x} = \frac{x - \bar{x}}{\sigma_x}$, being $\tilde{x}$ the data x normalized, $\tilde{x} = \mu_{RIDX,Predicted} - \mu_{RIDX,Measured}$, $\bar{x}$ the mean of x and σ_x its standard deviation. The Kolmogorov distribution is $K = \sup_{t \in [0,1]} |B(t)|$, $B(t)$ is the

Brownian bridge and the cumulative distribution of K is $Pr(K \leq x) = 1 - 2\sum_{k=1}^{\infty}(-1)^{k-1}e^{-2k^2x^2} = \frac{\sqrt{2\pi}}{x}\sum_{k=1}^{\infty}e^{-(2k-1)^2\pi^2/(8x^2)}$. The non-parametric Wilcoxon singed-ranked test uses the W statistic defined as $W = \sum_{i=1}^{N_r}[sgn(x_{2,i} - x_{1,i})]R_i$, where R_i denotes the pair rank starting with the smallest non-zero pair difference. For the flooded transition probability matrix, a paired-sample t-test testing the null hypothesis $H_0: \mu_{RIDX,Predicted} = \mu_{RIDX,Measured}$ at the 5% significance level was performed. This test was found appropriate because the differences between the $RIDX_{i,measured}$ and $RIDX_{i,predicted}$ were normally distributed when performing a non-parametric one-sample Kolmogorov-Smirnov test, testing the same hypothesis in the non-flooded Markov chain. The statistic used in the one-paired t-test is defined as $t = \frac{\bar{x}-\mu_0}{\frac{s}{\sqrt{n}}}$, being $\bar{x}$ the sample mean, μ_0 the value to be tested, s the sample standard deviation and n the sample size.

The transition probability matrices were validated once no statistical difference was found to reject the null hypothesis, which considers that the average values of predicted condition estimated from the Markov model equal the average measured condition. To test these hypotheses, a significant level of 5% was considered.

3.3 Quantifying the impact of flood in pavement deterioration

To quantify the impact of flooding on pavement deterioration, the research considered different questions.

1. Does the flood impact pavement deterioration?
2. How can we model the deterioration induced by flooding?
3. How can we quantify the consequences of flooding?

An illustrative flowchart was developed to graphically show this methodological process (*Figure 3*).

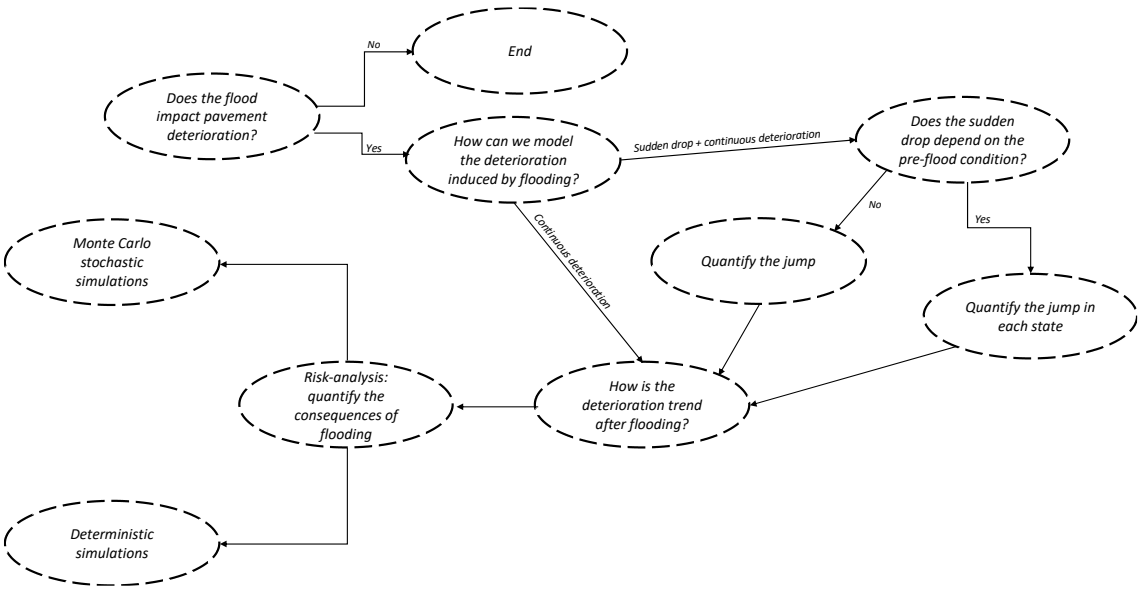

Figure 3: Flowchart for flooding deterioration quantification

The reader should bear in mind the asymptotic tendency and therefore, not accurate predictions a deterministic Markov process shows when the input condition index is within the two worst average state values. The deterministic approach predicts the $RIDX_{i+1}$ (*Eq 12*).

$$RIDX_{i+1} = [v_{i,1}, \dots, v_{i,n}] \cdot \begin{bmatrix} x_{1,1} & \cdots & x_{1,n} \\ \vdots & \ddots & \vdots \\ x_{n,1} & \cdots & x_{n,n} \end{bmatrix} \cdot \begin{bmatrix} \mu_1 \\ \vdots \\ \mu_n \end{bmatrix} \quad \textit{(Eq 12)}$$

The vector form $[v_{i,1}, \dots, v_{i,n}]$ transforms $RIDX_i$ to a vector such that $\sum_{j=1}^{n} v_{i,j} = 1$ and $v_{i,k} = 1 \Leftrightarrow RIDX_i = \mu_{k,f}$. This asymptotic and unrealistic behavior arises when the vector form $[v_{i,1}, \dots, v_{i,n}] \rightarrow [0, \dots, x_{n-1}, x_n]$, where $x_{n-1} + x_n = 1$. The Markov chain development tend to $\lim_{i \to \infty} [v_{\infty,1}, \dots, v_{\infty,n}] = [1,0, \dots,0]$ and therefore $RIDX_{t \to \infty} = \mu_n$, where μ_n is the last average state value of the corresponding transition probability matrix. However, the actual pavement deterioration reached indeed the worst condition always within a finite period of time. However, the author considered to disregard predicted deterministic values such that $RIDX < A_{s,end-1}$, where $A_{s,end-1}$ represents the penultimate state boundary, for all the statistical tests performed to justify the differences amongst deterioration rates for the flooded and non-flooded pavements. For the 5 state transition probability matrices using equal-length state conditions for $0 \leq RIDX \leq 100$, $A_{s,end-1} = 20$ and hence predictions where $RIDX_{predicted} < 20$ were disregarded. Note that predictions above the average best state condition are also unrealistic because for $RIDX_i > \mu_1 \Longrightarrow [v_{i,1}, \dots, v_{i,n}] = [1, \dots,0] \Longrightarrow RIDX_{i+1} = K$, where $K = ctt = [x_{1,1}, \dots, x_{1,n}] \cdot \begin{bmatrix} \mu_1 \\ \vdots \\ \mu_n \end{bmatrix}$.

3.3.1 Does the flood impact pavement deterioration?

The goal of this section was to determine if the flood event impacted the deterioration. As described in the literature review by several authors (Gaspard et al., 2007; Helali et al., 2008; Sultana et al., 2018b; Zhang et al., 2008) the flood had an impact on pavement performance, however, providing statistically-based justifications for the methodology proposed in this current study provided stronger shreds of evidences using different research approaches.

To achieve that a non-parametric Wilcoxon signed-ranked test was performed to compare the mean differences between the measured deterioration in the flooded sections and the results predicted by the non-flooded transition probability matrix obtained in the same sections from 2014 to 2018 testing the null hypothesis at the 5% significance level $H_0: \mu_{\Delta RIDX,Measured} = \mu_{\Delta RIDX,Predicted}$, being $\Delta RIDX_j = RIDX_{Year,i+1,j} - RIDX_{Year,i,j}$. The rejection of the null hypothesis allows to determine the flood impact the pavement deterioration but did not provide enough information to guarantee the behavior and trend. This test was found appropriate after carrying out a one-sample Kolmogorov-Smirnov test testing the null hypothesis $H_0: \mu_{\Delta RIDX,Measured} - \mu_{\Delta RIDX,Predicted} = 0$ at the 5% significance level.

3.3.2 How can we model the deterioration induced by flooding?

The current section targets the flooded pavement deterioration identification. Different deterioration processes were proposed and discussed amongst several alternatives. The methodology proposed analyzed statistically-based on each conceptual deterioration pattern to determine if the pattern could be rejected or not.

Four different conceptual types of deterioration are proposed (*Figure 4*). The first deterioration approach (*Figure 4a*) implied considering a delayed increase of deterioration due to the flooding over time with no substantial loss of condition when the flood occurs. The second deterioration approach (*Figure 4b*) suggested an important loss of the road condition when the flood occurs (i.e., jump in condition) but the flooded pavement follows a deterioration trend (i.e., slope) similar to the one of non-flooded sections. This model assumes that there is a "translation" (i.e., offset) of the deterioration curve driven by the initial jump. The third deterioration approach (*Figure 4c*) pointed to a combination of the first and second approaches. A rapid deterioration occurs when the flooding event occurs and a delayed increased deterioration of the flooded roads arises throughout the time. The fourth deterioration approach (*Figure 4d*) implies a sudden jump of the flooded roads but the condition tends to show no differences after a certain time, hence a slower deterioration trend arises for the flooded sections.

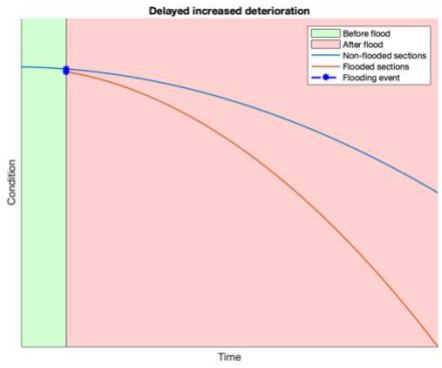

a. Conceptual deterioration I

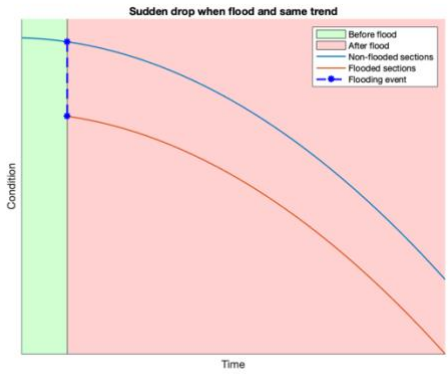

b. Conceptual deterioration II

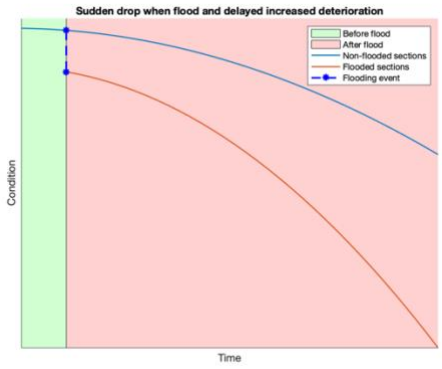

c. Conceptual deterioration III

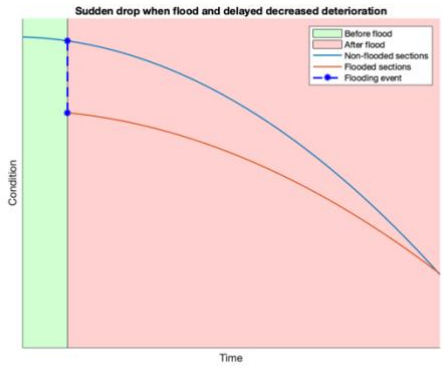

d. Conceptual deterioration IV

Figure 4: Conceptual deteriorations. a) Sudden drop and same trend. b) Sudden drop and increased deterioration. trend. c) Sudden drop and delayed decreased trend. d) Delayed increased trend.

With these conceptual models in mind, the thesis analyzed the actual deterioration of flooded pavements and compared it with an estimated deterioration that considered that the pavement was not flooded. This estimated deterioration was performed applying the non-flooded transition probability matrix over the flooded sections. The different conceptual models were analyzed using statistical analysis that seeks to respond to the following questions.

1. Is there a sudden drop in the pavement condition right after the flood?
    a. If the sudden drop exists, then the model depicted in (Figure 4a) is not adequate and discarded from the next analysis.
        i. If there is a sudden drop in the condition in the first post-flood measurement, does it depend on the pre-flood condition?
            1. If the sudden drop depends on the pre-flood condition, a quantification of the drop for each state is required.
            2. If the sudden drop is constant a single quantification of the drop is measured.
    b. If the sudden drop does not exist, then the model depicted in (Figure 4a) is the deterioration model because differences amongst deterioration rates were already found previously. Considering the flood impact cannot improve or slow the deterioration rate in the imminent post-flood measurement, the only feasible conceptual model is a delayed increased deterioration rate. Comparing the transition probability matrices strength and justifies this hypothesis by showing higher deterioration rates in the flooded transition probability matrix.

2. How is the deterioration after flooding? If a sudden drop exists
    a. If the flooded and non-flooded probability transition matrices showed no difference in their state-evolution probabilities, the conceptual deterioration is the one depicted in (*Figure 4b*).
    b. If the flooded transition probability matrix showed faster deterioration rates, hence higher probabilities to decrease its current state condition, the deterioration model is the one proposed in (*Figure 4c*).
    c. If the flooded transition probability matrix showed slower deterioration rates, the conceptual deterioration model is the one depicted in (Figure 4d).

3.3.3 Does the sudden drop exist?

The first analysis conveyed the need to determine the existence or not of a sudden decrease in condition after the first year of flooding. The existence of it allowed the author to disregard the model shown depicted in (Figure 4d) and discussed the remaining deterioration processes.

To determine statistically-based the existence of a sudden drop from the pre-flood measurement in 2013 and the first post-flood measurement in 2014 a non-parametric Wilcoxon signed-ranked test was performed to compare the differences between the

variation measured in the flooded sections and the variations predicted by the non-flooded transition probability matrix obtained in the same between 2013 and 2014 testing the null hypothesis at the 5% significance level $H_0: \mu_{\Delta RIDX,13-14,Measured} = \mu_{\Delta RIDX,13-14,Predicted}$. The rejection of the null hypothesis allowed to determine the flood slope variation just after the flood was different than the non-flooded sections, hence a sudden condition loss occurs during the first year. This test was found appropriate after carrying out a one-sample Kolmogorov-Smirnov test testing the null hypothesis $H_0: \mu_{\Delta RIDX,13-14,Measured} - \mu_{\Delta RIDX,13-14,Predicted} = 0$ at the 5% significance level.

3.3.3.1 Does the sudden drop depend on the pre-flood condition?

In this part, an analysis researching whether the sudden drop of condition when the flood occurs depends on the pre-flood condition. The sudden loss of condition $\delta(RIDX_i)$ was measured as $\delta(RIDX_i) = RIDX_{predicted,i} - RIDX_{measured,i}$ for the first year after the flood, typically $i = 1$, and its quantification allowed more precise simulations and accurate results for a risk-based analysis.

To determine statistically if either the drop when the flood occurs depends on the initial state or not, a non-parametric Kruskal-Wallis test was found to be appropriate for testing whether samples are originated from the same distribution. The samples used for the grouping sequence in the Kruskal-Wallis test were segregated according to their pre-flood condition, classifying them into their pre-flood state. In essence, 4 groups were analyzed, these ranging from states 2 to 5. $RIDX_{predicted,i} < 20$ were disregarded hence state 1 was not included in the analysis. The null hypothesis H_0 tested if the data in each state came from the same distribution using a 5%.

$$\begin{aligned} H_0: \mu_{\Delta RIDX,13-14,Measured,State,i} - \mu_{\Delta RIDX,13-14,Predicted,State,i} \\ = \mu_{\Delta RIDX,13-14,Measured,State,i+1} - \mu_{\Delta RIDX,13-14,Predicted,State,i+1} = \cdots \\ = \mu_{\Delta RIDX,13-14,Measured,State,nk} - \mu_{\Delta RIDX,13-14,Predicted,State,nk} \end{aligned}$$

The statistic used in this test H, is tested against $k - 1$ degree of freedom using the chi-square distribution, being k the number of different states. The statistic H is computed as $H = \frac{12}{N(N+1)} \sum \frac{R_i^2}{n_i} - 3(N+1)$ where N is the total number of observations, n_i is the number of observations in the *i*-th group, and R_i is the total sum of ranks in the *i*-th group.

The *p-value* returned was less than 0.05, the null hypothesis was rejected and hence the sudden drop depends on the pre-flood condition. Finally, the mean values, the number of observations, and the corresponding standard deviation for each state were collected.

3.3.4 How is the deterioration trend after flooding?

The deterioration trend analysis allowed to identify the trend flooded sections and non-flooded sections followed once the sudden drop occurred. Comparing the transition

probability matrices, using exclusively post-flood (i.e 2014-2018) data to calibrate the flooded probability matrix and pre-flood and post-flood data (i.e 2013-2018) was done to assess the deterioration trend. The Markov matrix for the flooded sections did not contain 2013 data because of the sudden drop identified modeled as a discontinuous deterioration, and the inclusion of the jump would modify the deterioration trend, which is continuous. It is important to note that due to the discontinuity the jump provokes data in the best states may not be found and hence the transition probability matrix was calibrated for every state but used finally for states 1, 2, and 3.

3.4 Risk analysis: quantifying the consequences of flooding in pavement condition

Risk analysis to quantify the flood impact over the network was carried out in this part. Two different approaches were set and critically discussed: a stochastic approach using the Monte Carlo method and a deterministic deterioration evolution, where no randomness was linked to the flooded sections. These analyses were found to be suitable for assessing the loss of life condition the flooded sections had compared to the non-flooded evolution.

The first analysis was based on applying stochastic Monte Carlo simulations over the non-flooded transition probability matrix. This approach allowed capturing the randomness associate with pavement deterioration. A limitation using this stochastic risk analysis arises when the overall pavement condition can only take the average state value of the corresponding matrix. The average state value was estimated by the 50th percentile of data observed in the corresponding state. In the cases where the state did not vary in more than a consecutive year a linear discretization throughout the state in each simulation was carried out rather than maintaining the constant average state value.

The 10th, 50th, and 90th percentiles using the non-flooded transition probability matrix were simulated. The Monte Carlo method was found to be consistent when there is a clear asymptotic tendency measuring the accumulated average deterioration index, and this determines the number of required simulations. Once the non-flooded percentiles were obtained two different approaches are used to simulate the risk-based analysis over the flooding sections: a stochastic approach and a deterministic one.

3.4.1 Monte Carlo Method approach

Monte Carlo simulations were performed to determine the deterioration curves in the non-flooded sections and the deterioration curves corresponding to its 10th, 50th, and 90th percentiles are obtained. A uniform probability distribution was considered to develop the simulations.

To evaluate and quantify the flood impact, a flooded simulation for every different state "n" was performed, where $2 \leq n \leq 5$. The starting point was computed as $RIDX_{0,n}$ (*Eq 13*), where $\mu_{n,\mathrm{n}f}$ is the flooded average state value for the state "n" and $RIDX_{i,p}$ the $RIDX$ for a given year "i" included in the percentile p deterioration curve. A single

evaluation for each state was carried out based on this premise which in turn gives the most realistic simulation for a given state due to its proximity to the average state value.

$$RIDX_{0,n} = RIDX_{i,p} = \min_{\forall i} \left| \mu_{n,\mathrm{n}f} - RIDX_{i,p} \right| \qquad \textit{(Eq 13)}$$

For the flooded simulations, the first post-flood measurement $RIDX_{1,n}$ considered that the sudden drop when the flood occurs, whose value depends on its initial state, was applied after running a deterministic case applying the non-flooded transition probability matrix (*Eq 14*) starting from $RIDX_{0,n}$.

$$RIDX_{1,n} = \left[v_{0,1}, \dots, v_{0,nk} \right] \cdot \begin{bmatrix} x_{1,1,nf} & \cdots & x_{1,nk,nf} \\ \vdots & \ddots & \vdots \\ x_{nk,1,nf} & \cdots & x_{nk,nk,nf} \end{bmatrix} \cdot \begin{bmatrix} \mu_{1,\mathrm{n}f} \\ \vdots \\ \mu_{nk,\mathrm{n}f} \end{bmatrix} - \delta\left(RIDX_{1,n}\right) \qquad \textit{(Eq 14)}$$

Where $RIDX_{1,n}$ is the first post-flood condition at year $i = 1$, $\left[v_{0,1}, \dots, v_{0,n} \right]$ the pre-flood vector form at year $i = 0$, $\begin{bmatrix} x_{1,1,nf} & \cdots & x_{1,nk,nf} \\ \vdots & \ddots & \vdots \\ x_{nk,1,nf} & \cdots & x_{nk,nk,nf} \end{bmatrix}$ the non-flooded transition probability matrix, where $nk = \max(n)$, $\begin{bmatrix} \mu_{1,\mathrm{n}f} \\ \vdots \\ \mu_{nk,\mathrm{n}f} \end{bmatrix}$ the corresponding average state vector and, $\delta\left(RIDX_{1,n}\right)$ the sudden loss of condition due to the flood for the state "n".

A linear deterioration within the same state was carried out when the condition state did not vary for more than a year. Otherwise, it took the average state value. The linearization provided a vectorial $RIDX_n$ for a given state using (*Eq 15*) or (*Eq 16*).

$$RIDX(i, \dots, i+k)_n = A_{state} + \frac{B_{state} - A_{state}}{k+1} \cdot (1, \dots, k) \underset{if\ only}{\Longleftrightarrow} k > 0 \vee nr = n \in RIDX_{1,n} \qquad \textit{(Eq 15)}$$

$$RIDX(i)_n = \mu_{nr,f} \underset{if\ only}{\Longleftrightarrow} k = 0 \ \wedge \ nr \neq n \in RIDX_{1,n} \qquad \textit{(Eq 16)}$$

A_{state} is the corresponding state lower boundary, and B_{state} the upper boundary, i the time-step where $RIDX$ is analyzed and $i + k$ the last time-step $RIDX(i, \dots, i+k)$ has not yet downgrade its n state, and i the first time-step assessed in n. The reader should note whereas A_{state} took the lower state value except in the lowest state where it took the average state value, B_{state} took the upper boundary except when $RIDX_{i=1,n}$ (Eq 17). Otherwise, B_{state} takes the upper boundary of the state n.

$$B_{state} = RIDX_{i,n} \underset{if\ only}{\Longleftrightarrow} i = 1 \qquad \textit{(Eq 17)}$$

Note that $B_{state}\left(RIDX_{0,n}\right) \underset{if\ only}{\Longleftrightarrow} A_{state} \leq RIDX_{1,n} \leq B_{state}$. The main limitation applying this approach was found when the sudden drop led to a deterioration index just after flooding close to the lower state boundary. The stochastic simulations were not able to recognize the probability to change to the next state depends on the condition after the jump but it considered the probability to change based on the

deterioration index corresponding to the upper state boundary. To address this issue, a temporary modification over the transition probability matrix was performed for the post-drop state condition to the flooded transition probability matrix. For a generic transition probability matrix TPM (*Eq 18*).

$$TPM = \begin{bmatrix} x_{1,1} & \cdots & x_{1,nk} \\ \vdots & \ddots & \vdots \\ x_{nk,1} & \cdots & x_{nk,nk} \end{bmatrix} \quad \textit{(Eq 18)}$$

When assessing $RIDX_{1,n}$, the corresponding n row $[x_{n,1}, \dots, x_{n,k}, x_{n,k+1}, \dots, x_{n,nk}]$ is transformed to.

$$[x_{n,1}, \dots, x_{n,k} \cdot \frac{B_{n(RIDX_{t-1})} - A_n}{\Delta_n}, x_{n,k+1}, x_{n,k+1} \cdot \frac{x_{n,k} \cdot \left(1 - \frac{B_{n_{(RIDX_{t-1})}} - A_n}{\Delta_n}\right)}{\sum_{j=k+1}^{nk} x_j}, \dots, x_{n,nk} + x_{n,nk} \cdot \frac{x_{n,k} \cdot \left(1 - \frac{B_{n_{(RIDX_{t-1})}} - A_n}{\Delta_n}\right)}{\sum_{j=k+1}^{nk} x_j}]$$

Where $\Delta_n = \frac{100}{\mathrm{nk}}$ for $n < \mathrm{nk}$ and $\Delta_n = A_{n-1} - \mu_{n,f}$ for $n = \mathrm{nk}$ where $\mu_{nk,f}$ is the worst average state value for the flooded transition probability matrix.

This approach allowed to capture how far from the end of the state $RIDX_{1,n}$ is located and reassigned the whole interval probabilities whereas the state condition remains in the post-flood state using a linear approach. Otherwise, inconsistencies assessing the yearly $RIDX$ arose. Monte Carlo simulations were run beginning on $RIDX_{1,n}$ and the different deterioration curves were obtained. The results to be analyzed are the paired 10^{th}-10^{th} percentiles for the flooded and non-flooded results and the 50^{th}-50^{th} and 90^{th}-90^{th} percentiles.

This analysis allowed to compare the expected deterioration, the 50^{th} percentiles of both sections, and the extreme deterioration rates, 10^{th} and 90^{th} percentiles, simultaneously. The main insights of the analysis allowed to determine, in percentage and absolute value, the loss of life for the fastest, slowest, and mean deterioration rates for both flooded and non-flooded sections.

3.4.2 Deterministic approach

The deterministic approach proposed was based on applying the flooded transition probability matrix beginning in $RIDX_1$ after the flood occurs. The analysis was performed for the 10^{th}, 50^{th}, and 90^{th} percentile of the non-flooded transition probability matrix results and assessed in each state. The starting point for each case was also determined according to (*Eq 13*).

The main limitation of applying this approach was found when the deterioration enters the second-to-last state. In this case, the vector form tends asymptotically to the last average state value and cannot perform the deterioration evolution over the second-to-last state.

This analysis allowed to determine the loss of expected life according to the flood year since the road was constructed without including randomness to the flooded

deterioration. Hence, it was possible to determine how the flooded sections assimilated to a given non-flooded percentile deterioration rate.

4 RESULTS

The current section shows the case-study results from the proposed methodology.

4.1 Identification of flooded and non-flooded pavements

Shapefiles from the different counties containing geographical identification were merged and 21,381 observations were found. Once filtered by route section "*ROUTE"*, reference point "*REFPT*" and end reference point "*ENDREFPT*" according to the data available in the dataset containing the deterioration measurements, the number of observations was reduced to 17,784. The next filter applied was the removal of concrete and composite pavements which accounted for 2,755 observations. Road sections without flood hazard zone assigned were found to be 1,461. Every section contained precipitation data and functional class. A total of 13,568 sections remained and the total final miles in were reduced from 1,939 to 1,099 miles. The miles observed in each family "*Precipitation-Flooding Risk Zone*" are shown in (*Table 2*).

		Flooding Risk Zone		
		No Risk	Moderate-High Risk	Very High Risk
Precipitation registered	No/Few Precipitation	**363.22**	7.49	2.61
	Moderate Precipitation	437.44	10.69	3.58
	Heavy Precipitation	250.94	9.13	**14.44**

Table 2: Miles registered in different flood-precipitation zones regardless functional class

As expected from good engineering road design practices, most sections were located over "*1. Area of minimal flood hazard*", representing 1,051.6 miles, and only 20.6 miles on a "*4. Floodway*". Regarding the precipitation, 373.3 miles were located within the "*1. No/few Precipitation*" category whereas 274.5 miles over the "*3. Heavy Precipitation*". The precipitation histogram is shown in (*Figure 5*).

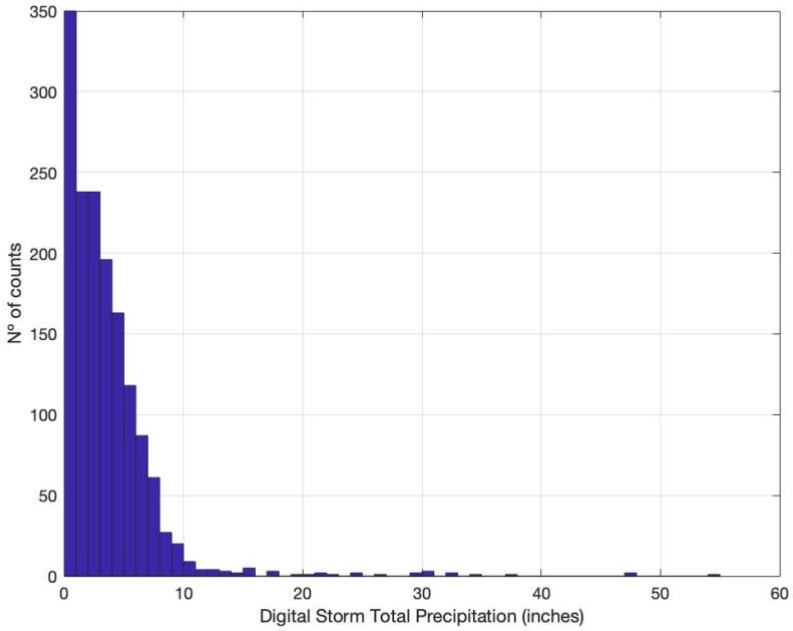

Figure 5: Precipitation histogram

Disregarding the AADT levels the numbers a total of 63 families were found. In (*Figure 6*).

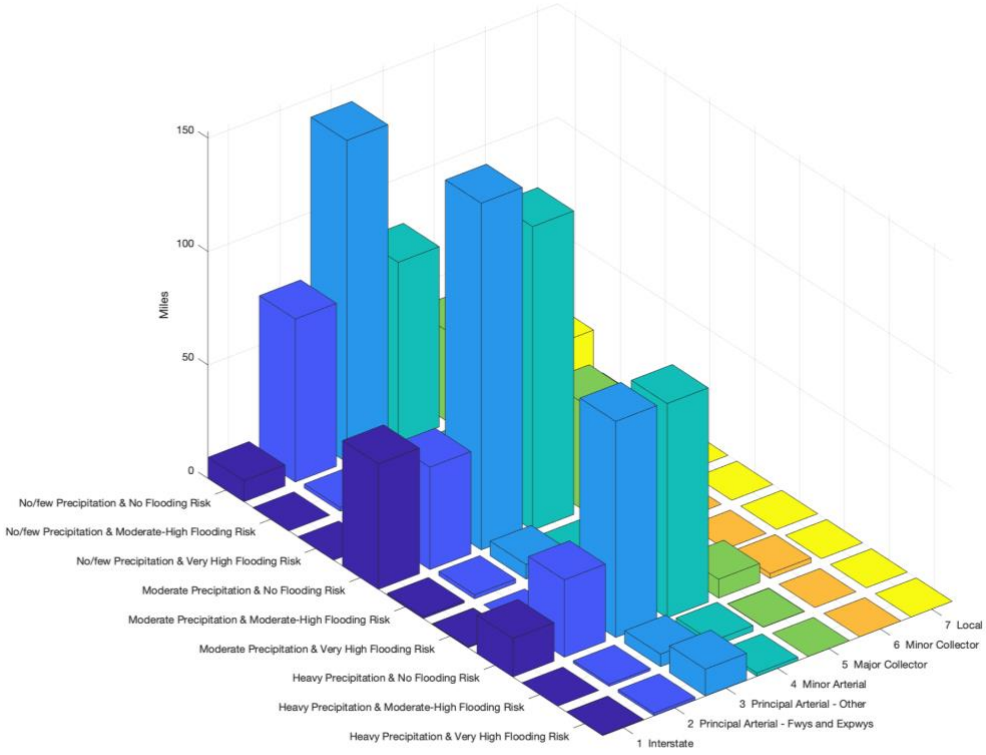

Figure 6: Miles registered in each family

Pavement sections in the "3. *Principal Arterial - Other*" functional class were selected for the study due to the relatively small variability in the AADT (*Figure 7*) and the high quantity of miles in the selected counties. The outliers of the dataset, computed the lower as $Outliers_{low} = Q1 - 1.5IQR$ and the upper as $Outliers_{upp} = Q3 + 1.5IQR$, being $Q1$ and $Q3$ the 25th and 75th percentiles of the AADT distribution and $IQR = Q3 - Q1$, were found to satisfy $1 \cdot 10^4 < AADT < 2 \cdot 10^4$. At the same time, the functional class "3. *Principal Arterial - Other*" had the most flooded sections (*Figure 6*).

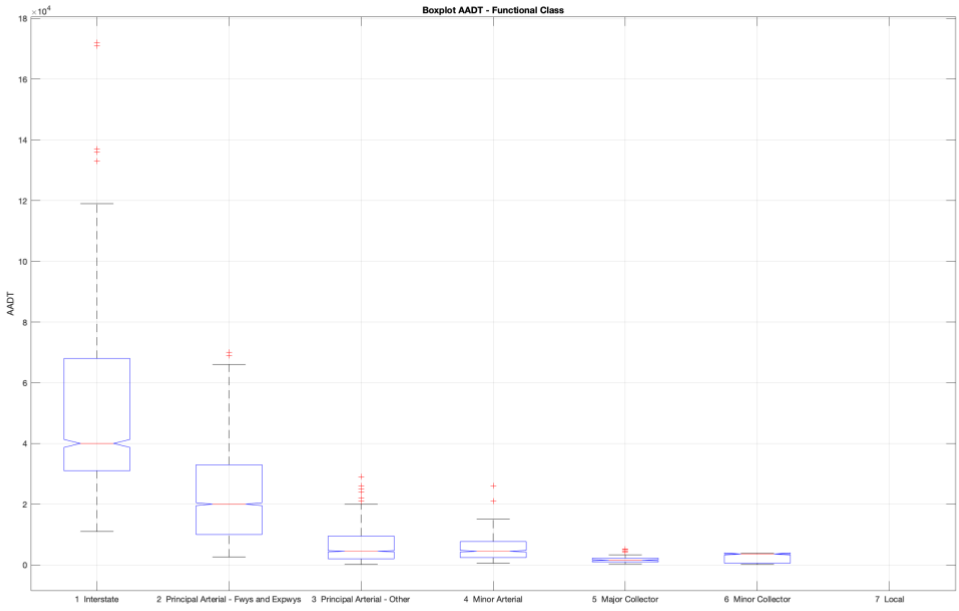

Figure 7: AADT – Functional Class boxplots

An overall of 153.57 miles for the "*3. Principal Arterial – Other*" functional class contained the dataset before filtering, which could be segregated amongst 141.80 miles for the non-flooded sections and 11.77 miles for the flooded sections. The overall miles contained in each family for "*3. Principal Arterial – Other*" functional class is shown in (*Table 3*).

		Flooding Risk Zone		
		No Risk	**Moderate-High Risk**	**Very High Risk**
Precipitation registered	**No/Few Precipitation**	**141.80**	3.63	1.51
	Moderate Precipitation	152.75	6.44	2.08
	Heavy Precipitation	95.21	5.52	**11.77**

Table 3: Miles registered in different flood-precipitation zones for functional class "3. Principal Arterial – Other"

4.2 Development and validation of pavement deterioration models for flooded and non-flooded models

Sections not including continuous measurements from 2013 to 2018 were excluded from the analysis for consistency. This action reduced the maintenance dataset from 14,117 to 12,798 data points. These data points were then analyzed to identify cases of registered maintenance, unregistered maintenance, and anomalies. For modeling the pavement performance, sections that were treated/rehabilitated and therefore its condition improved are no longer under consideration. Otherwise, modeling pavement performance using this data would provide unrealistic results.

Registered maintenance: maintenance treatments recorded in the *Bid Analysis and Management System* (BAMS) dataset from *CDOT* was used to identify segments receiving treatments. Generally, there was a clear improvement in the IRI condition in the sections found to be rehabilitated and they are no longer considered in the analysis. All the rehabilitations were assessed to verify the rehabilitation had improved the IRI condition. Generally, there was a clear improvement in the IRI condition in the sections found to be rehabilitated and they are no longer considered in the analysis. All the rehabilitations were assessed to verify the rehabilitation had improved the IRI condition. Sections were reduced from 12,798 to 10,923.

For the unregistered maintenance observations were reduced from 10,923 to 5,659. Analogously, the anomalies detected reduced the dataset from 5,659 to 4,941. That led to an overall 1,930 remaining sections in 2013 (9.5% reduction), 1,187 in 2014 (44.3% reduction), 814 in 2015 (61.8% reduction), 590 in 2016 (72.3% reduction), 247 in 2017 (88.4% reduction) and 173 in 2018 (91.8% reduction). Most of the sections were from the non-flooded family, counting 1,822 in 2013, 1,126 in 2014, 766 in 2015, 558 in 2016, 235 in 2017 and 163 in 2018. The flooded sections contained 108 sections in 2013, 61 in 2014, 48 in 2015, 32 in 2016, 12 in 2017 and 10 in 2018. A bar graph depicts the section evolution in (*Figure 8*).

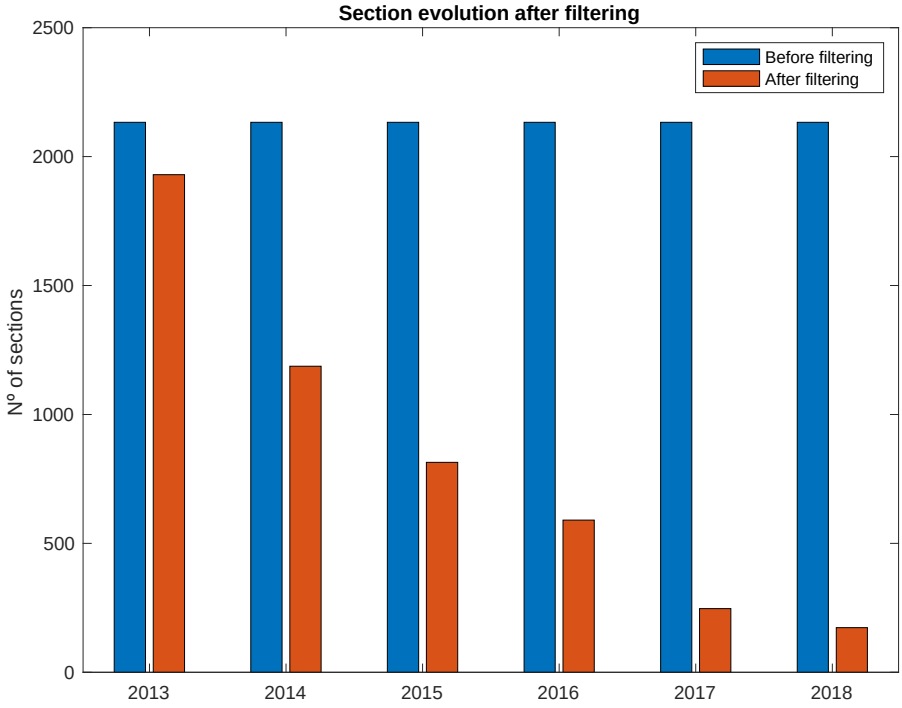

Figure 8: Section evolution after filtering

The transition probability matrices were developed using equidistant states ranging from a standardized index of 0 to 100 (*Figure 9*). Different approaches accounting for assessing the IRI without any transformation (*Eq 19*) were found to be unable to validate the transition probability matrices due to extreme IRI values that led to states with few observations and large intervals.

$$RIDX_{IRI} = IRI \qquad \textit{(Eq 19)}$$

To reduce problems found in the extreme values, a non-linear sigmoidal function (*Eq 20*) to predict the $RIDX$ was also tested. Different slopes were tested in the sigmoidal function such that $k = \lambda \cdot i$ with $\lambda = 0.002$ and $i = 1,2,\dots,50$ However, most slopes were unable to provide statistical validation varying greatly with the random points used in the validation test, and the different $RMSE$ were found not to be stable for small slope variations, hence this approximation was disregarded. These problems arose because the function provides a steep slope when the IRI is close to x_0 and a very smooth $\Delta RIDX_{sig}$ when the IRI is far from x_0, where x_0 was defined as the 50th percentile of the IRI found in the condition dataset.

$$RIDX_{sig} = \frac{100}{1 + e^{k(IRI - x_0)}} \qquad \textit{(Eq 20)}$$

The use of 6 or more states led to the impossibility to gather data in some states, hence they were no longer considered due to the impossibility to derive the discrete-time Markov chain in every state. The results here discussed are focused on developing a 5-

state probability matrix for both flooded and non-flooded sections using (*Eq 21*) as a deterioration index.

$$RIDX = 100 - \frac{IRI - \min(IRI)}{\max(IRI) - \min(IRI)} \qquad \textit{(Eq 21)}$$

Cases over the 90th percentile, which implies IRI values over 223 inch/mile were disregarded from the analysis. The linear standardized index (*Eq 21*) used to analyze the pavement condition takes values of $RIDX = 100$ for an $IRI = 26$, which was the lowest IRI value found in the dataset. Analogously, when $IRI = 223 \longrightarrow RIDX = 0$.

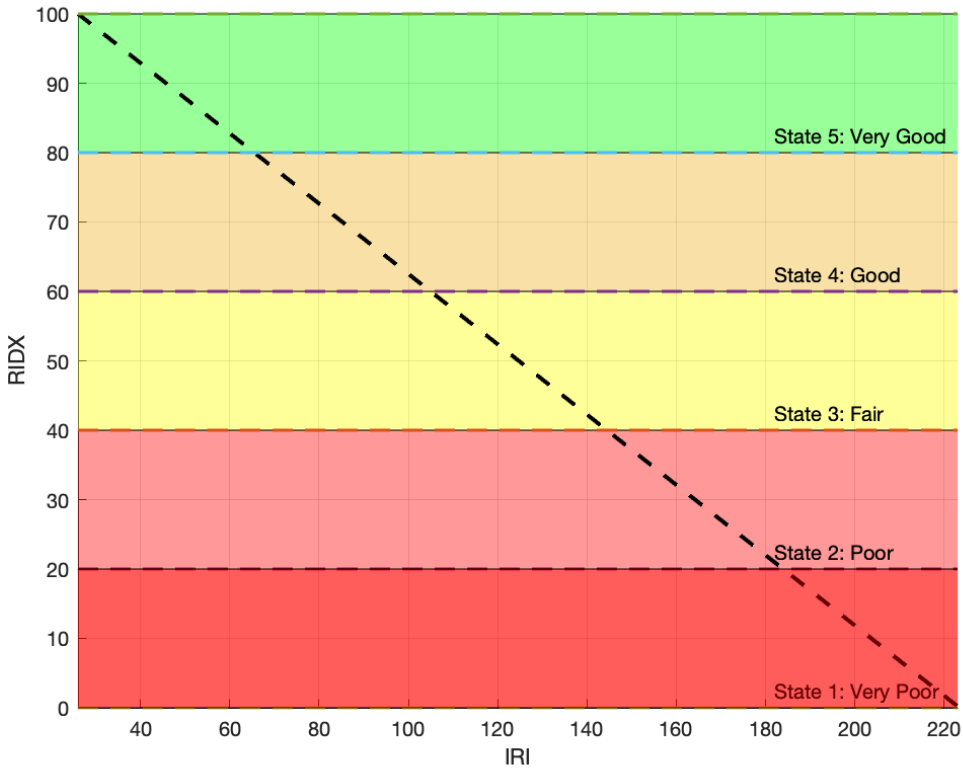

Figure 9: Standardized RIDX

The discrete-time Markov chain used a 1-year timeframe interval. Due to the anomalies and maintenances registered the overall data points used to develop the matrices were not continuous over time and only continuous data is used. 2,072 transitions are found for the non-flooded sections and 112 cases for the flooded sections.

4.2.1 Deterioration of non-flooded pavements

For the non-flooded case, the transition probability matrix took the following state intervals $[100-80, 80-60, 60-40, 40-20, 20-0]$ with an average state, assessed as the 50th percentile of the IRI in each state $[84.80, 70.11, 51.37, 31.61, 11.86]$. The percentages of cases registered in each state were $[24.11, 34.32, 26.13, 12.53, 2.90]$ being them all consistent, where >10% in each

state for a 5-state transition probability matrix, according to (Pérez-Acebo et al., 2019). States thresholds and extreme boundaries, corresponding to $RIDX = [100, 80, 60, 40, 20, 0]$ correspond to $IRI(\frac{inch}{mile}) = [26, 60, 105, 144, 183, 223]$. From a conceptual point of view the states corresponded to a "*Very Good*", "*Good*", "*Fair*", "*Poor*" and "*Very Poor*" conditions.

The transition probability matrix is represented in (*Figure 10*). The transition probability matrix described the probability of one segment to transition from a given state to a different state in one year. Based on the results obtained, non-flooded pavements in very good condition (state 5), for example, have a 0.574 probability to stay in this same state after one year, and a 0.360 probability to transition to a "*Good*" condition (state 4).

$$TPM_{non-flooded} = \begin{bmatrix} & \#5 & \#4 & \#3 & \#2 & \#1 \\ \#5 & 0.574 & 0.360 & 0.047 & 0.018 & 0.000 \\ \#4 & & 0.587 & 0.317 & 0.073 & 0.028 \\ \#3 & & & 0.496 & 0.366 & 0.137 \\ \#2 & & & & 0.588 & 0.412 \\ \#1 & & & & & 1.000 \end{bmatrix}$$

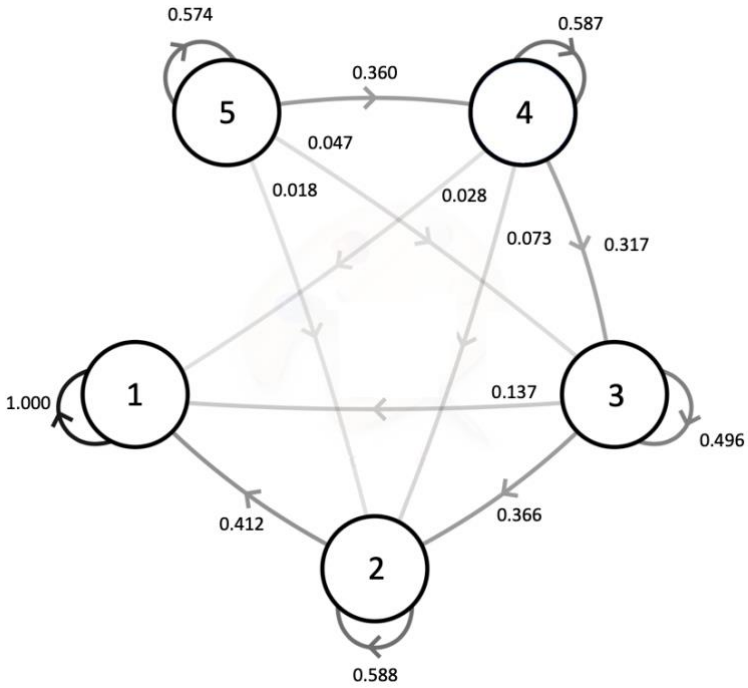

Figure 10: Homogeneous Markov chains for non-flooded sections

The filters applied restraining anomalies and maintenance have limitations and did not capture all the IRI improvements. 70 cases were found to improve pavement performance in the calibration set and 13 in the validation. These cases have been disregarded for consistent analyses. The suggestion of having at least 10% of the observations in each state for 5-state Markov chain (Pérez-Acebo et al., 2019) is fulfilled except in the worst condition state but it was not found not relevant for assessing the trend because once the lowest condition state is reached, there are no more possible

transitions. Hence, once the worst state is reached, the Markov chain is not able to provide more insights on pavement deterioration.

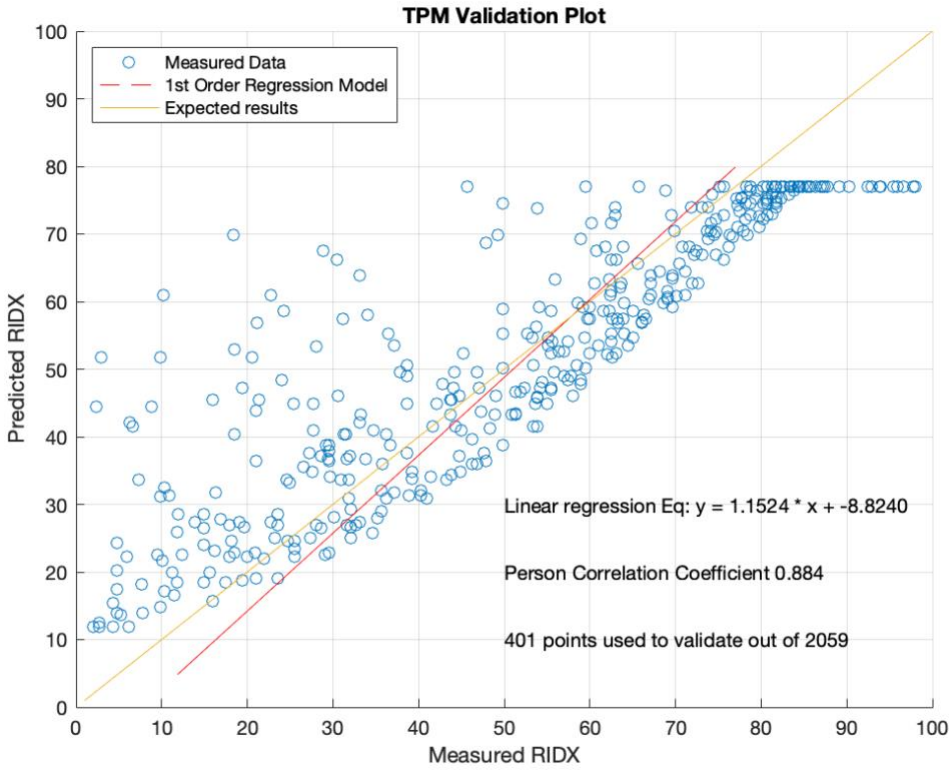

Figure 11: Validation set for the non-flooded transition probability matrix

From the validation plot (*Figure 11*), a $RMSE = 0.90$ is obtained, tested over 401 points and obtaining a Pearson's correlation coefficient $\rho_{X,Y} = \frac{COV(X,Y)}{\sigma_X \sigma_Y} = 0.884$, being X the measured $RIDX$ and Y the predicted $RIDX$. The Wilcoxon Signed-Rank test failed to reject the null hypothesis (p-value $0.168 > 0.05$). This allows us to conclude that no statistical difference was found between the predicted and measured $RIDX$, hence the transition probability matrix for non-flooded pavement is validated. The Wilcoxon Signed-Rank test was found to be appropriate because the difference between predicted and actual conditions was found to be not normal. This was determined from a One-Sample Kolmogorov-Smirnov test (p-value $7.19 \cdot 10^{-7} < 0.05$).

4.2.2 Deterioration of flooded pavements

For the flooded case the transition probability matrix took the same state values as the non-flooded with an average state, assessed as the 50th percentile of each state $[-, -, 47.83, 27.31, 12.87]$. The percentages of cases registered in each state are $[-, -, 41.86, 39.53, 11.63]$. Due to the sudden decrease of pavement condition after the flood, state nº4 "*Good*" and state nº5 "*Very Good*" were no longer possible, hence the transition probability matrix only made sense for state nº1 "*Very Poor*", nº2 "*Poor*" and nº3 "*Fair*". For graphical purposes, the transition probability matrix states were flipped and the non-flooded represented (*Figure 12*).

$$\mathrm{TPM}_{flooded} = \begin{bmatrix} & \#5 & \#4 & \#3 & \#2 & \#1 \\ \#5 & & & & & \\ \#4 & & & & & \\ \#3 & & & 0.389 & 0.389 & 0.222 \\ \#2 & & & & 0.588 & 0.412 \\ \#1 & & & & & 1.000 \end{bmatrix}$$

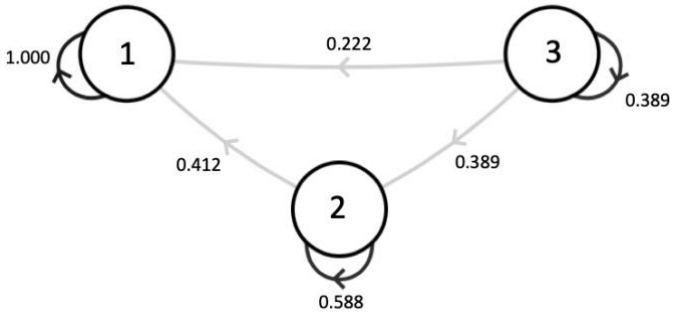

Figure 12: Homogeneous Markov chains for flooded sections

The suggestion of having at least 10% of the observations in each state for the 5-state Markov chain (Pérez-Acebo et al., 2019) was fulfilled in each valid state where the flooded transition probability matrix was applied. 1 case was found to improve pavement performance in the calibration set and 1 in the validation. These cases were disregarded for consistent analyses.

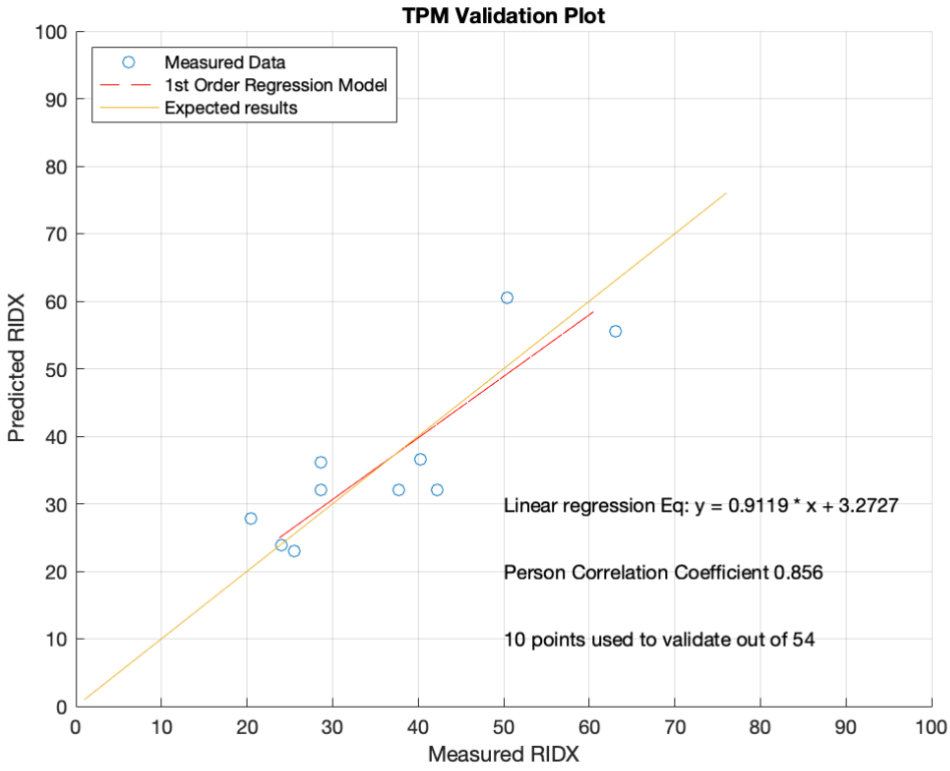

Figure 13: Validation set for the flooded transition probability matrix

From the validation plot (*Figure 13*) a $RMSE = 0.1025$ is obtained, tested over 10 points and obtaining a Pearson's correlation coefficient $\rho_{X,Y} = \frac{COV(X,Y)}{\sigma_X \sigma_Y} = 0.856$, being X the measured $RIDX$ and Y the predicted $RIDX$. The One-Sample T-Test test failed to reject the null hypothesis (p-value $0.964 > 0.05$). This allows concluding that no statistical difference was found between the predicted and measured $RIDX$, hence the transition probability matrix for flooded pavement is validated. The One-Sample T-Test was found to be appropriate because the difference between predicted and actual conditions was found to be normal. This was determined from a One-Sample Kolmogorov-Smirnov test (p-value $0.932 > 0.05$).

4.3 Quantifying the impact of flood in pavement deterioration

Predicted values $RIDX_{predicted} < 20$ were removed. Once the pavement condition reaches a "*Very Poor*" condition the analysis using deterministic approaches over the transition probability matrices were no longer realistic and the state evolution stagnant. Furthermore, there is no need to evaluate pavement for "*Very Poor*" conditions.

4.3.1 Does the flood impact pavement deterioration?

The non-parametric Wilcoxon signed-ranked test failed to reject the null hypothesis (p-value $0.01 < 0.05$). This test was found appropriate after carrying out a One-Sample Kolmogorov-Smirnov test where predicted and actual condition was found to be no normal (p-value $0.03 > 0.05$). Hence, the flood event impacts pavement deterioration, the deterioration rate was found to be different when comparing flooded and non-flooded sections.

4.3.2 How can we model the deterioration induced by flooding?

The T-Test found there was statistical evidence to determine that the deterioration rates during the first year using the non-flooded transition probability matrix over the flooded sections and the measured observations on the flooded sections were different (p-value $7.5 \cdot 10^{-4} < 0.05$). Hence, it was possible to model the flooded sections with a sudden drop measuring the pavement condition that occurs once the flood occurs. The T-Test was found to be suitable after performing a Kolmogorov-Smirnov (p-value $0.26 > 0.05$) failing to reject the null hypothesis the data came from a standard normal distribution.

4.3.2.1 Does the sudden drop depend on the pre-flood condition?

The Kruskal-Wallis test provided a *Chi-square* of 12.78, the statistic H is tested against $k - 1$ degree of freedom using the chi-square distribution, being $k = 4$ the number of different states ranging from 2 to 5 "*Poor*" to "*Very Good*". The Kruskal-Wallis test returned a p-value of $0.004 < 0.05$ which rejected the null hypothesis that the sudden drop considering the initial state came from the same distribution. Hence, it was possible to statistically determine that the sudden drop value depends on the pre-flood state. A comprehensive boxplot is developed in (*Figure 14*).

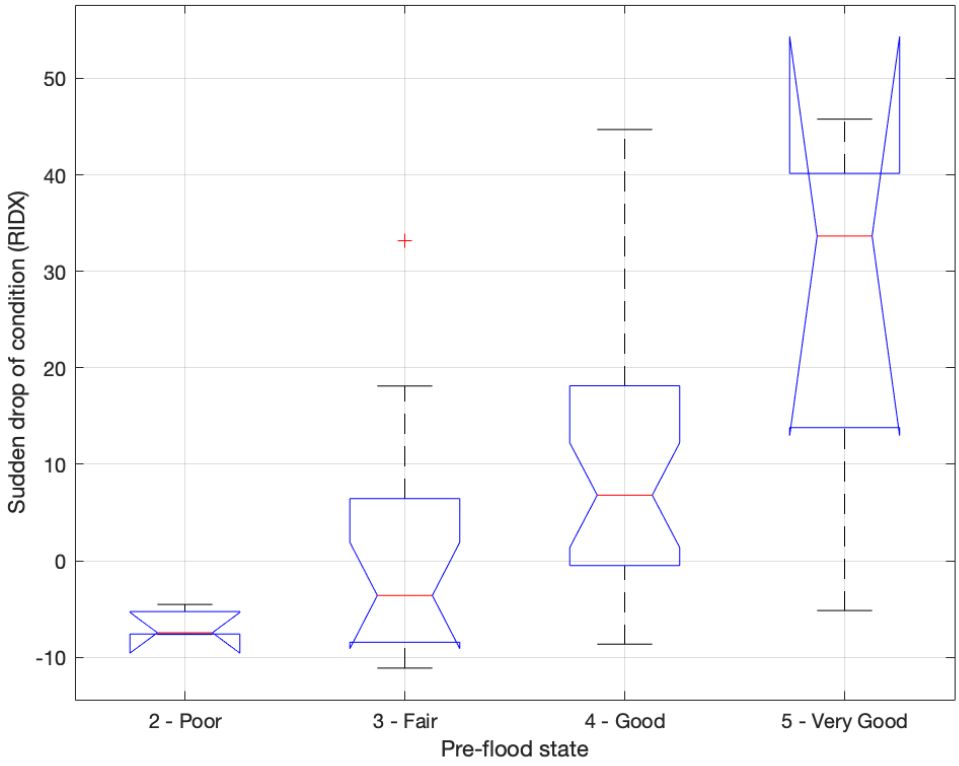

Figure 14: Sudden drop of condition according to its pre-flood state

The sudden mean drop was obtained averaging the state's drops taking values $\Delta RIDX_{Predicted-Measured}$ of -6.5, 0.5, 11.1, and 27.0 from states 2 to 5, respectively. The number of occurrences found was 3, 18, 29, and 4 and 1.7, 11.7, 14.9, and 22.2 its standard deviation from states 2 to 5, respectively. The results from state 2 "*Poor*" are inconsistent because an improvement was registered. The problem may arise from just having three observations and hence it will be considered no jump is recorded to state 2, similar to state 3 where the jump is very small and negligible. Note that assessing the drop along with state "*Very Poor*" had no sense for a post-development using the transition probability matrix. A correlation was also found assessing the Pearson Correlation Coefficient $\rho_{X,Y} = \frac{COV(X,Y)}{\sigma_X \sigma_Y} = 0.477$, being X the actual measured $RIDX$ in 2013 and Y the loss of condition due to the flood impact $RIDX_{Predicted,2014} - RIDX_{Measured,2014}$, which could be interpreted as a sudden drop, hence a sudden loss of pavement condition. The results are depicted in (*Figure 15*).

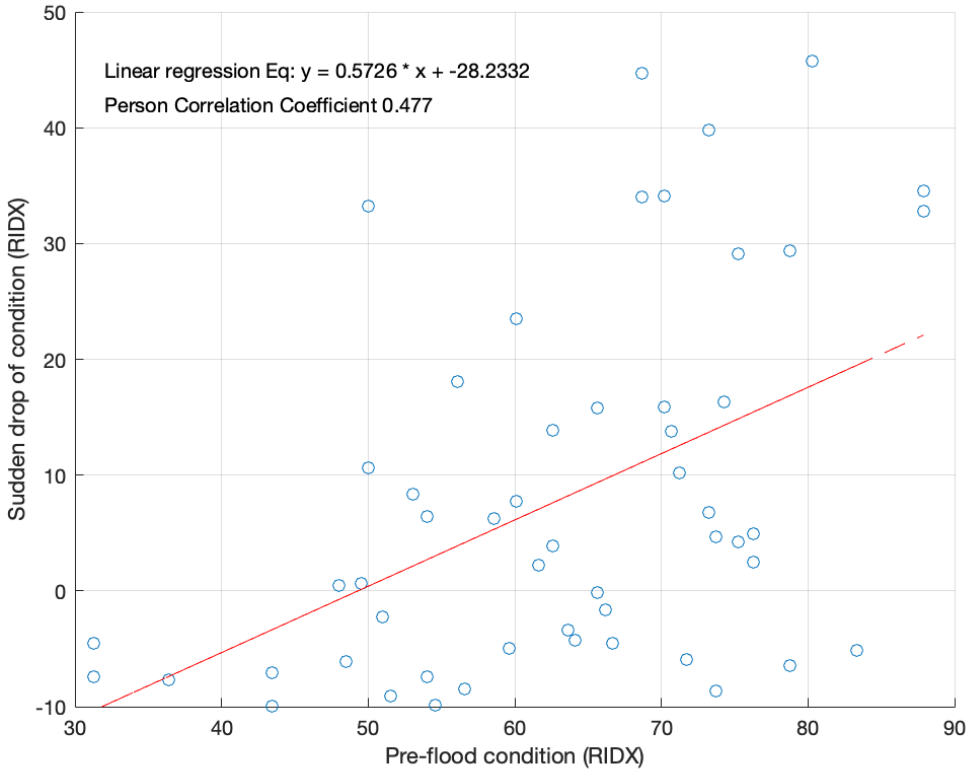

Figure 15: Sudden drop of condition regarding the pre-flood condition

4.3.3 How is the deterioration trend after flooding?

The best way to compare the deterioration trend after flooding was by comparing the different transition probability matrices. A slightly faster deterioration rate for state 3 was found for the flooded sections, whereas the same deterioration rate for state 2. These findings suggest when the pavement reached a "*Poor*" condition, in this case, state 2, there was no difference in the deterioration rate between flooded and non-flooded sections. The pavement had so much accumulated deterioration that the impact of the flood did not modify the performance, even a small sudden drop is found, taking $\Delta RIDX = 1.5$ which if disregarded small differences would be noticed.

$$\mathrm{TPM}_{non-flooded} = \begin{bmatrix} & \#5 & \#4 & \#3 & \#2 & \#1 \\ \#5 & 0.574 & 0.360 & 0.047 & 0.018 & 0.000 \\ \#4 & & 0.587 & 0.317 & 0.073 & 0.028 \\ \#3 & & & 0.496 & 0.366 & 0.137 \\ \#2 & & & & 0.588 & 0.412 \\ \#1 & & & & & 1.000 \end{bmatrix}$$

$$\mathrm{TPM}_{flooded} = \begin{bmatrix} & \#5 & \#4 & \#3 & \#2 & \#1 \\ \#5 & & & & & \\ \#4 & & & & & \\ \#3 & & & 0.389 & 0.389 & 0.222 \\ \#2 & & & & 0.588 & 0.412 \\ \#1 & & & & & 1.000 \end{bmatrix}$$

The difference amongst the transition probability matrices showed a slight increase in deterioration in the "*Fair*" state and no difference in the "*Poor*" state. Hence, the trend was only affected during the "*Fair*" state.

$$\mathrm{TPM}_{flooded} - \mathrm{TPM}_{non-flooded} = \begin{bmatrix} & \#5 & \#4 & \#3 & \#2 & \#1 \\ \#5 & & & & & \\ \#4 & & & & & \\ \#3 & & & -0.107 & 0.023 & 0.085 \\ \#2 & & & & 0.000 & 0.000 \\ \#1 & & & & & 0.000 \end{bmatrix}$$

A boxplot comparing the predicted deterioration (*P*) using the non-flooded transition probability matrix over the flooded sections and comparing these predictions with the actual measurements (*M*) was developed from 2013 to 2015 (*Figure 16*). A clear difference amongst the slopes in the first year was found whereas a very similar slope was noticed afterward from the first to the second year as expected when assessing the difference amongst the transition probability matrices. From 2016 to 2018 there were only 20, 7, and 3 measurements remaining which created inconsistent boxplot evolutions and hence have not been depicted in this study.

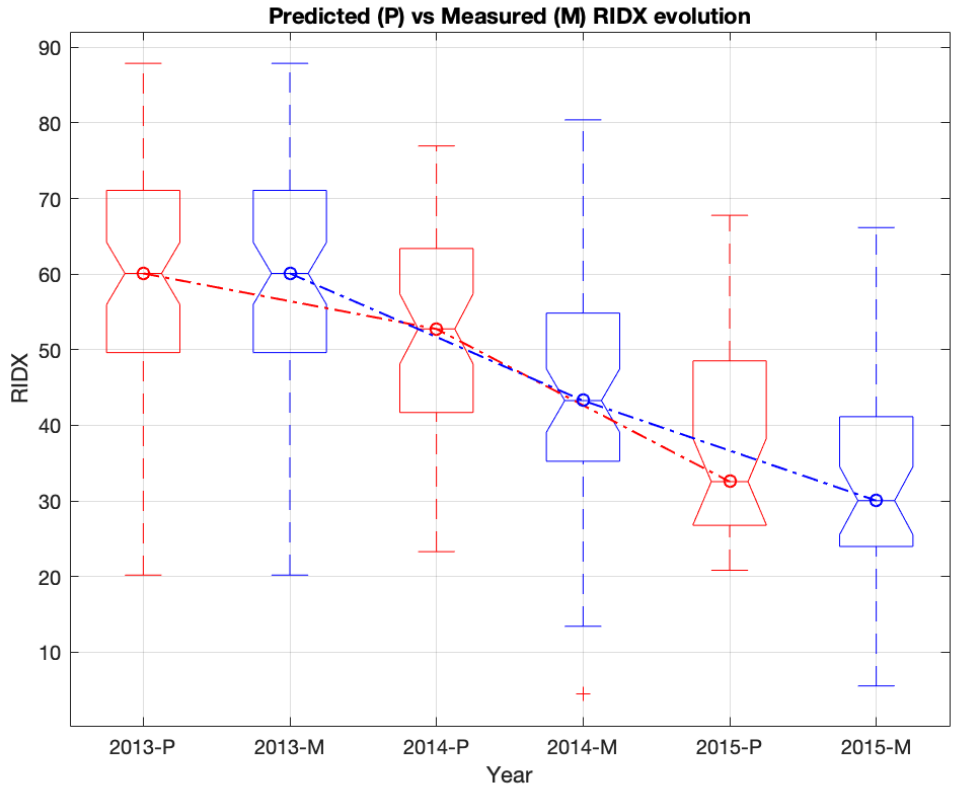

Figure 16: Predicted (P) and measured (M) section evolution

The deterministic boxplot approach was useful to determine the sudden drop, which was found in the flooded sections during the first year after the flood where the 25th, 50th and 75th percentiles of the flooded sections took significantly lower conditions,

which confirms the sudden loss of condition previously discussed, but it is noticeable when initial good IRI conditions were predominant as shown assessing the 25th, 50th and 75th percentile in 2013, the pre-flood condition.

The conceptual modeling evolution for the flooded sections becomes state-dependent when comparing the transition probability matrices. Due to the state-dependent condition, a faster deterioration is shown if the post-flood condition $RIDX_1$ is in state 3 "*Fair*", such that $40 < RIDX_1 < 60$ and the deterioration rate becomes stationary once condition reaches state 2 "*Poor*". With these premises a deterioration model when the pre-flood condition is above $RIDX_0 \geq 60$"*Good*" (*Figure 17*) or, alternatively when $RIDX_0 < 60$ the deterioration model is depicted in (*Figure 18*).

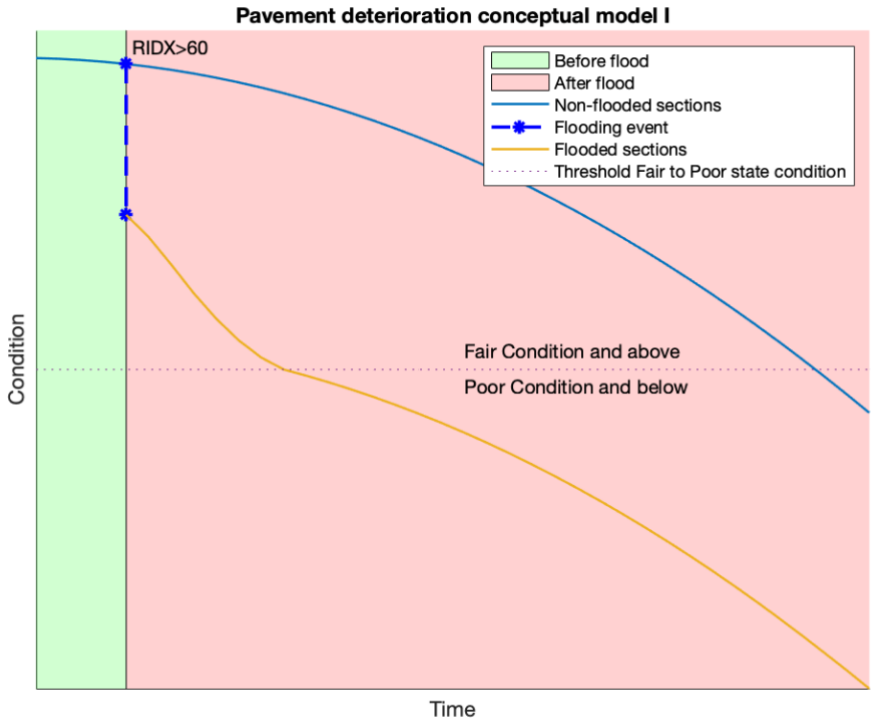

Figure 17: Deterioration when $40 < RIDX_1 < 60$ *and* $RIDX_0 \geq 60$

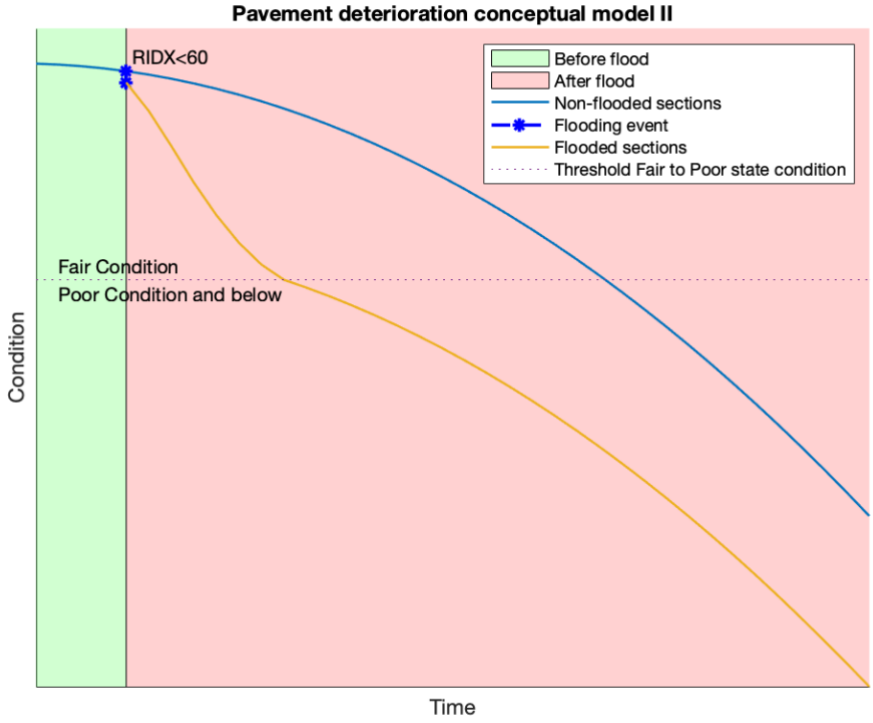

Figure 18: Deterioration when $40 < RIDX_1 < 60$ *and* $RIDX_0 < 60$

However, the deterioration rate after flooding is not modified if the $RIDX_1$ condition reaches state 2 "*Poor*", $20 < RIDX_1 < 40$, which conceptually can be modeled according to (*Figure 19*) if $RIDX_0 \geq 60$ or (*Figure 20*) if $RIDX_0 < 60$.

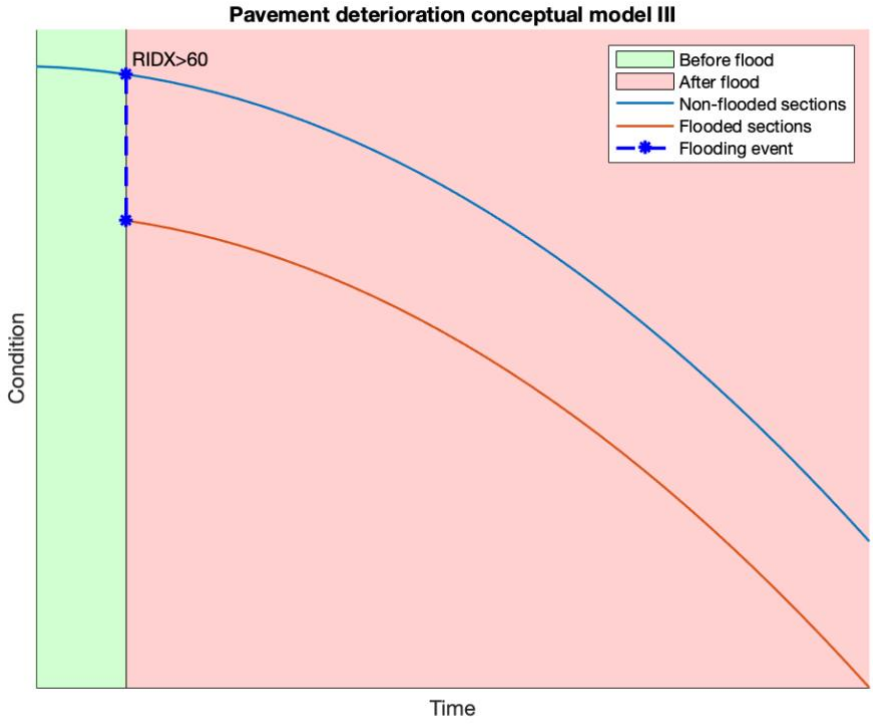

Figure 19: Deterioration when $20 < RIDX_1 < 40$ *and pre-flood condition* $RIDX_0 > 60$

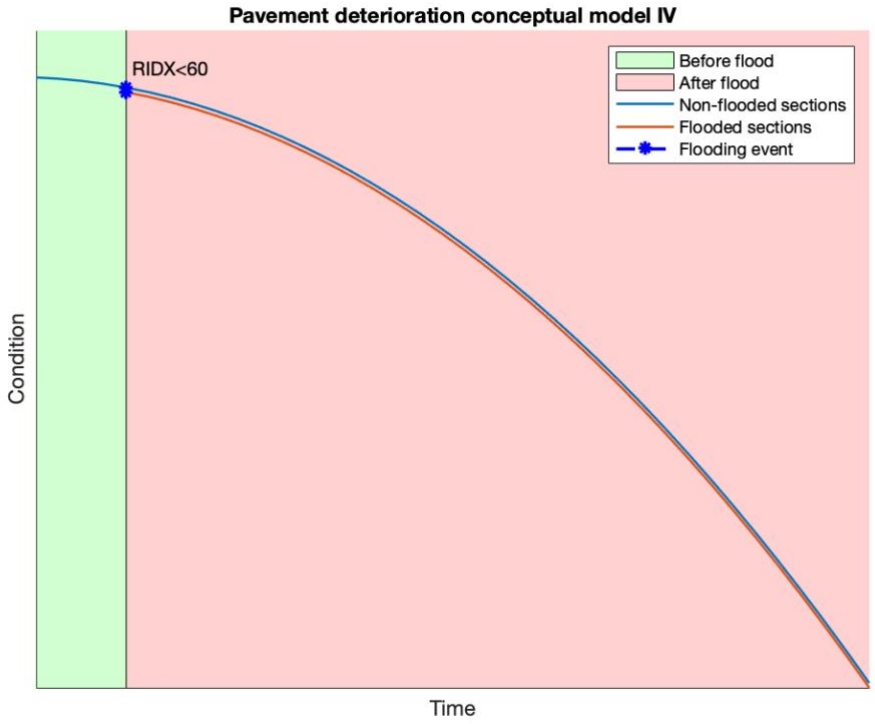

Figure 20: Deterioration when $20 < RIDX_1 < 40$ and pre-flood condition $RIDX_0 < 60$

The reader should note that when a deterministic approach is applied for values above the average vector best state value, $RIDX > 84.4$, the non-flooded transition probability matrix returns always a $RIDX = 77$, hence results above this RIDX does not deteriorate so fast and the results may be not realistic.

4.4 Risk analysis: quantifying the consequences of flooding in pavement condition

The main aim of developing a risk-based analysis was to investigate the loss of life due to the flood event. The loss of life was considered when the sections reach the last state 1, which corresponds to a "*Very Poor*" condition and is represented by values fulfilling $RIDX < 20$, corresponding to $IRI > 183\ inch/mile$. Analyses starting over the best $RIDX$ possible were developed, which simulate once the road was open to traffic once is constructed/fully rehabilitated.

Two different approaches were set. A first Monte Carlo approach allowed to compare the impact of the flood when comparing the same percentiles for both flooded and non-flooded sections, this can be understood as comparing a paired relationship between the highest, lowest, and expected deterioration rates for both sections. Alternatively, a deterministic approach provided insightful results when no randomness is associated to the flooded sections, allowing to how the expected deterioration of the flooded sections assimilates to the non-flooded regarding the three percentiles considered. Even though the same tendencies flooding and non-flooding follow from nearly state 3 downwards, due to $\forall i\ \mu_{i,nf} \neq \mu_{i,f}$, in the different figures shown, especially when assessing

percentiles, the deterioration values may not coincide showing similar trends but shifted.

4.4.1 Monte Carlo Method approach

10,000 simulations for the Monte Carlo method were developed to obtain the non-flooded 10th, 50th, and 90th percentiles. 10,000 Monte Carlo simulations were further developed for the flooding case for each state and the 10th, 50th, and 90th non-flooded percentiles. The analyses were focused on the 10% fastest and slowest deterioration rates corresponding to the 10th and 90th percentiles, respectively.

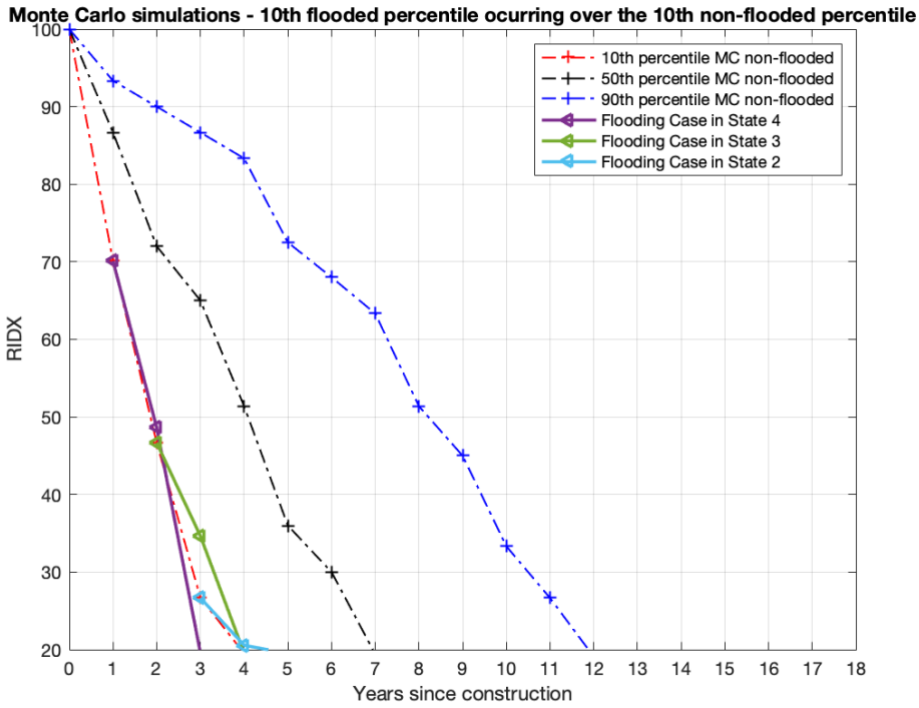

Figure 21: Monte Carlo simulations for the 10th percentile

The 10th percentile, showing the 10% fastest deterioration rate, shows a loss of life in the flooded sections compared to the non-flooded of 1.00 years, 0.00 years, and 0.00 years, corresponding to a loss of 25%, 0.0%, and 0.0% for the state 4, state 3 and state 2, respectively (*Figure 21*). Note that in this case, a pre-flood state with "*Very Good*" condition was not able to be developed because $RIDX_{year0} = 100$, $RIDX_{year1} = 70$ and the average non-flood state condition $\mu_{5,\mathrm{n}f} = 84.40$ for a state $80 < RIDX_{state,5} < 100$.

The reader should note that the state 2 curve starts showing an asymptotic tendency around $RIDX = 20$ and the expected results should derive the same tendency the non-flooded section follows. However, it is important to remark that $\mu_{nk,nf} < \mu_{nk,f}$, but it is considered that no loss of life is reported because $RIDX_7 \cong 20$ for state 2. This drawback is common but the valuable data is not the tendency below $RIDX < 20$ but the loss of life.

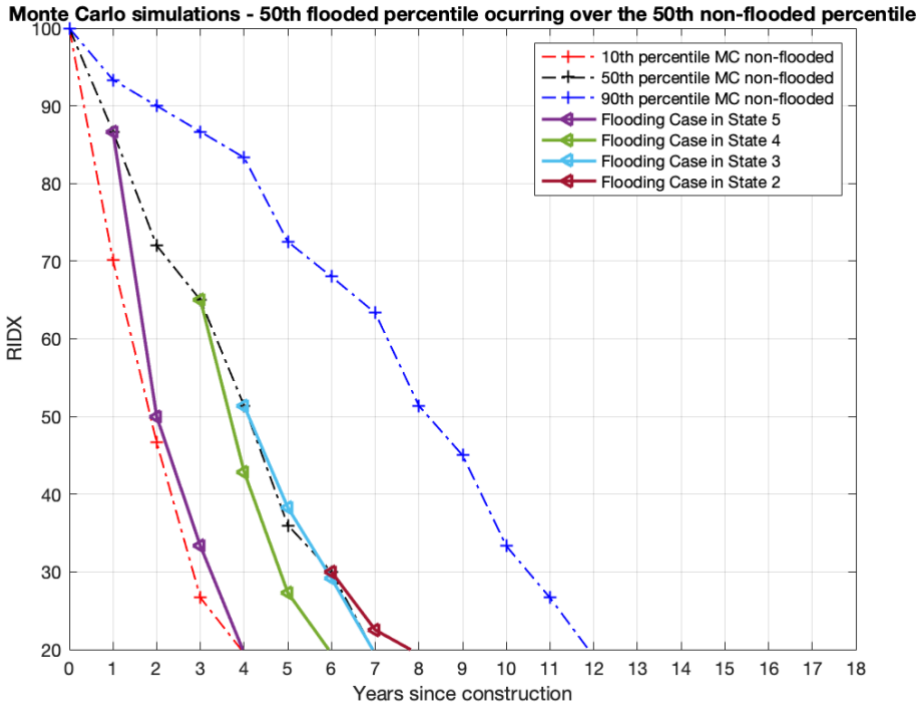

Figure 22: Monte Carlo simulations for the 50th percentile

The 50th percentile, corresponding to the expected deterioration, simulated a loss of life in the flooded roads contrasted to the non-flooded of 3.00 years, 1.00 years, 0.00 years, and 0.00 years, corresponding to a loss of 42.9%, 14.3%, 0.00%, and 0.0% for states 5 to 2, respectively (*Figure 22*). State 2 shows the same problem as the 10th percentile.

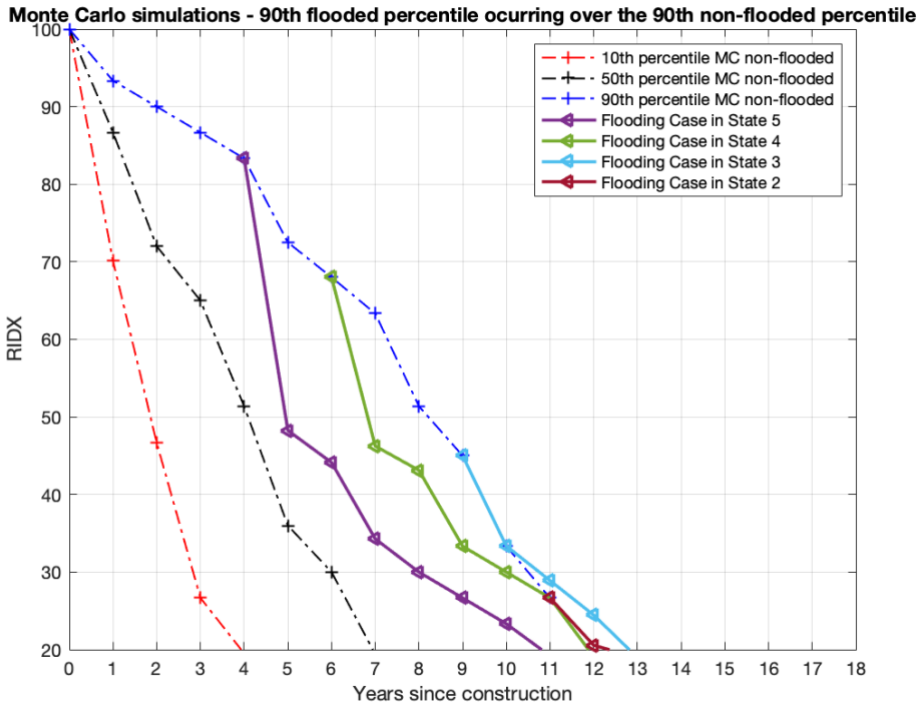

Figure 23: Monte Carlo simulations for the 90th percentile

The 90th percentile exhibits a loss of life in the flooded segments to the non-flooded of 1.25 years, 0.00 years, -0.00 years, and -0.00 years, corresponding to a loss of 10.4%, 0.0%, 0.00%, and 0.00% for states ranging from 5 to 2, respectively (*Figure 23*). This case for states 4 to 2 shows the shifting problem due to different $\forall i\ \mu_{i,nf} \neq \mu_{i,f}$. However, the results are still consistent and the small losses of life are disregarded. A summary of the Monte Carlo simulations is shown in (*Table 4*).

		Percentile					
		10%		50%		90%	
State	2 - Poor	0.0%	0.00	0.0%	0.00	0.0%	0.00
	3 - Fair	0.0%	0.00	0.0%	0.00	0.0%	0.00
	4 – Good	25.0%	1.00	14.3%	1.00	0.0%	0.00
	5 – Very Good	N/A	N/A	42.9%	3.00	10.4%	1.25

Table 4: Loss of pavement life using Monte Carlo simulations (left: loss of life in %, right: loss of life in years)

The stochastic approach showed a reduction of pavement life is expected for "*Good*" and "*Very Good*" pavement conditions, and the same deterioration for "*Fair*" and "*Poor*" condition, hence the flood increases the deterioration in asphalt pavements depending on its pre-flood condition, the better the pavement condition the higher the deterioration. The expected mean deterioration for both flooded and non-flooded sections (*Figure 22*), assessing in both sections the 50th percentile, provides a dramatic decrease of pavement condition when the pre-flood condition is "*Very Good*" up to 42.9%. Even it has not been feasible to verify it for the 10th fastest percentile, the transition probability matrix suggests an even higher loss of condition, in percentage, would be expected for the 10th percentile. The results showed no flood impact when the pre-flood condition is either "*Fair*" or "Poor", these results were expected because both transition probability matrices were very similar for the "*Poor*" condition and a negligible sudden drop was found for "*Fair*" pre-flood condition and no drop for the "*Poor*".

4.4.2 Deterministic approach

The deterministic evolution was applied over the 10th, 50th, and 90th percentiles obtained from the non-flooded sections stochastic simulations. In order to provide the most accurate results, the deterministic starting point in each state was selected as the closest $RIDX$ to the non-flooded average state value for the selected percentile. This approach allowed to capture the flood impact when no randomness is associated with the flooded sections in comparison to the 10th, 50th and 90th percentiles when randomness is included in the non-flooded pavements.

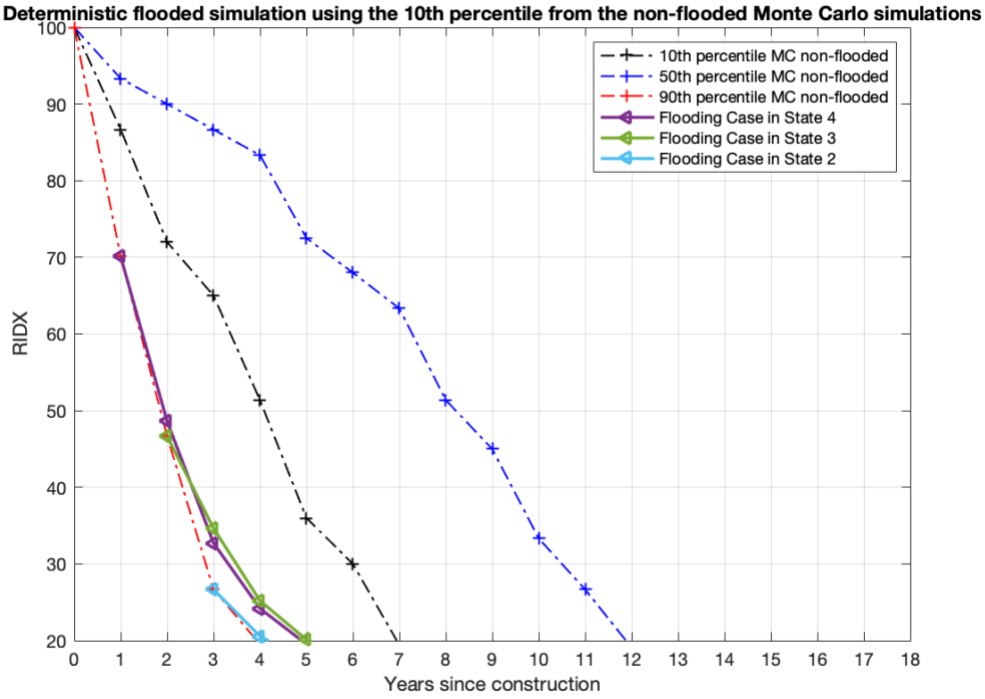

Figure 24: Deterministic flooded evolution over the 10th stochastic non-flooded percentile

The deterministic approach showed the expected deterioration due to the flooding practically follows the same deterioration trend the 10th non-flooded percentile does. Comparing the results to the 10th non-flooded percentile a loss of life of -1.00 years, -1.00 years, and 0.00 years is expected (*Figure 24*) for states 4 to 2, respectively. The state "*Very Good*" was not included for the same reasons exposed in the Monte Carlo analysis over the 90th percentile.

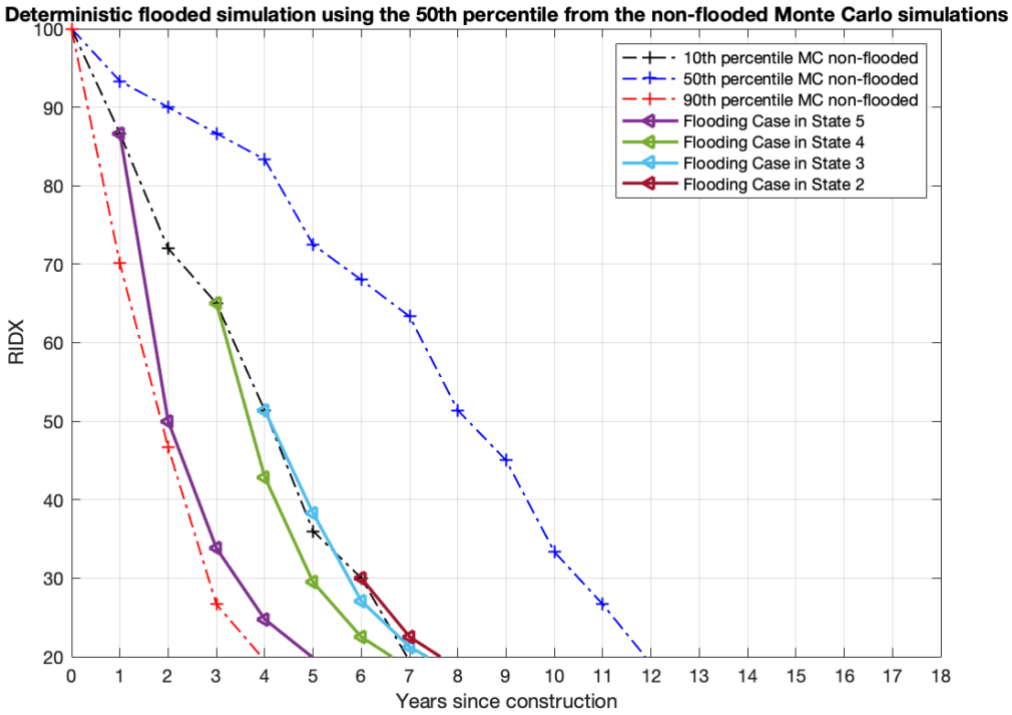

Figure 25: Deterministic flooded evolution over the 50th stochastic non-flooded percentile

A loss of life of 2.00 years, 0.50 years, 0.00 years, and 0.00 years is expected when comparing the deterministic results over the expected non-flooded deterioration, corresponding to 28.6%, 7.1%, 0.0%, and 0.0% from states 5 to 2, respectively. These results exhibited the pre-flood condition impact over the loss of life (*Figure 25*).

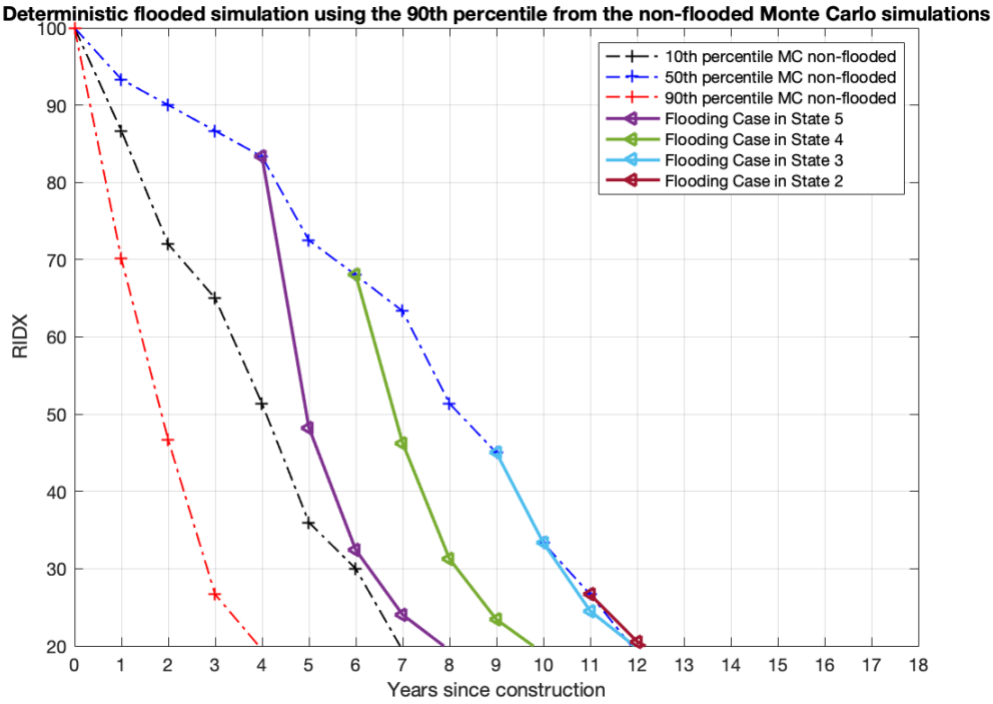

Figure 26: Deterministic flooded evolution over the 90th stochastic non-flooded percentile

Finally, a loss of 4.00 years, 2.25 years, 0.00 years, and 0.00 years, corresponding to a loss of life of 33.3%, 18.8%, 0.0%, and 0.0% from state 5 to 2, respectively, is expected when applying the transition probability matrix over the 10% slowest non-flooded deterioration rate. A summary of the results is exhibited in (*Table 5*).

		Percentile					
		10%		50%		90%	
State	2 - Poor	0.0%	0.00	0.0%	0.00	0.0%	0.00
	3 - Fair	-25.0%	-1.00	0.0%	0.00	0.0%	0.00
	4 – Good	-25.0%	-1.00	7.1%	0.50	18.8%	2.25
	5 – Very Good	N/A	N/A	28.6%	2.00	33.3%	4.00

Table 5: Loss of pavement life using a deterministic approach (left: loss of life in %, right: loss of life in years)

The findings of this approach show that when no randomness is involved in the flooded deterioration, the flooded sections deteriorate as the 50th flooded percentile for "*Fair*" condition, which means there is no flood impact. Nevertheless, the tendency shows a shift to the 10th percentile to "*Good*" and "*Very Good*" conditions, meaning a considerable flood impact. The increased deterioration due to flooding in the network is reported with these findings, and maintenance costs are likely to increase to recover the same pavement condition. The overall maintenance and administration expenditure are going to increase when the sections are flooded.

5 CONCLUSIONS, LIMITATIONS AND FUTURE RESEARCH

5.1 Conclusions

The purpose of this study was to determine and quantify the impact of flooding on the pavement condition of asphalt roads. This study analyzed the floods impacting Colorado in 2013 and developed deterioration models for non-flooded and flooded pavements using homogeneous Markov chains and Monte Carlo simulation to quantify the flood impact in terms of IRI.

As reported by (Gaspard et al., 2019, 2007; Helali et al., 2008; Sultana et al., 2016c) the study revealed the flood affected negatively the pavement condition, however, it is possible to identify that from a "*Fair*" condition upwards only.

The current research reveals the deterioration of flooded pavement can be modeled according to its pre-flood and post-flood conditions. The findings show a sudden loss of condition in the first year of the flood when the pre-flood condition is "*Good*" or "*Very Good*". Otherwise, there is a negligible or no relevant sudden drop of condition. The deterioration trend is found to slightly increase for the flooded sections along with the "*Fair*" state but the same trend is found when it reaches a "*Poor*" state.

Analyzing the stochastic Monte Carlo simulations important pavement condition losses arises in every single percentile analyzed. The expected deterioration, which was found analyzing the 50th percentile from the Monte Carlo simulations, was translated into a loss of the expected pavement life of 42.9% for the flooded sections when the pre-flood condition was "*Very Good*", 14.3% for "*Good*" and no reduction is reported for "*Fair*" and "*Poor*" conditions. The deterministic approach suggests the flooded pavements, when no randomness is considered, deteriorates as the 50th percentile of non-flooded sections for "*Poor*" and "*Fair*" condition but it gradually shifts to the 10th percentile when the pre-flood condition is improved. Comparisons among stochastic and deterministic analyses are consistent and interdependent. The stochastic allows quantifying the deterioration rates probabilistically using the 10th, 50th, and 90th percentiles whereas the deterministic shows how no randomness in flooded sections tends to tilt from the 50th to 10th non-flooded percentile when the pre-flood condition increases.

The results of this research support the ideas that the flood reduces pavement stiffness (Gaspard et al., 2007) and that once the water from the flood is drained, the stiffness is recovered (Asadi et al., 2020; Nazarian and Yuan, 2012; Yu-Shan and Shakiba, 2021). This research contributes to the body of knowledge by providing insights into the conceptual deterioration of flooded pavements and a particular application in Colorado.

The results found in this case study showed that sections with a poor and below pre-flood conditions ($RIDX < 40$ and $IRI > 144$) suffer no impact by the flood and when analyzing a fair condition ($40 < RIDX < 60$ and $144 > IRI > 105$) very small impact is reported in the transition probability matrix. However, the stochastic approach showed no relevant loss of life is expected for $RIDX < 60$. These results were aligned with the literature (Sultana et al., 2016c; Lu et al., 2018; Texas Department of

Transportation, 2019) during the flood and further post-flood recovery activities, highly loaded emergency vehicles are expected to increase these already flood-affected pavements.

This new understanding of the impact of floods in pavement conditions will help transportation agencies in the design of resilience programs and post-flood strategies. The corresponding DOT should propose the use of roads whose $IRI > 144$ to avoid the loss of deterioration due to the flood for these heavily loaded vehicles carrying mainly debris or $IRI > 105$ to expect very little loss in pavement deterioration due to the flood. When the emergency tasks are carried out pavement saturation is very high and hence an important decrease of its stiffness modulus is expected for roads in good and very good condition, bringing a larger condition loss and translated into higher maintenance costs shortly. As highlighted by (Khan et al., 2017a) this research also wants to emphasize the importance of post-flood strategies to minimize the increased deterioration due to the flood. These findings suggest that in general the pavement age plays a key role and the oldest roads should be designated for the emergency vehicle routes. Infrastructure asset managers should include flood uncertainty forecasting higher budget expenditures according to the results obtained in the current study.

5.2 Limitations and future research

The major limitations of this study are the lack of pavement structure data, pavement age, and the lack of significant flooded observations from 2016 onwards. However, good engineering practices led to construct roads over non-floodway regions, and proper infrastructure asset management will consider rehabilitating the flooded sections that suffered most in a brief period of time. The latter may point to consider the flood impact could be even greater because the study filtered the sections to check no rehabilitation was carried out after the flood, which presumably were the most affected ones. In spite of its limitations, the study certainly adds to our understanding of pavement management and deterioration rates when a flood occurs.

The homogeneous Markov-chains used in the study are calibrated for a given functional class and geographical location. Whilst this study did not confirm the transition probability matrices can be applied to other road types and regions, it certainly described a methodological process to calibrate them and consider flood modeling.

A natural progression of this work is to analyze the pavement thickness influence and the environmental attributes. Another issue not addressed in this study was the pavement saturation content and its influence need of further investigation. New research analyzing other flood events using similar methodologies to understand the influence of different flood characteristics, location, and climate conditions in this phenomenon would be the next steps.

5.3 Conflict of interests

The author declares no conflict of interest.

6 BIBLIOGRAPHY

Achebe, J., Oyediji, O., Saari, R.K., Tighe, S., Nasir, F., 2021. Incorporating Flood Hazards into Pavement Sustainability Assessment. Transp. Res. Rec. 03611981211014525. https://doi.org/10.1177/03611981211014525

Al-Omari, B., Darter, M.I., 1995. Effect of Pavement Deterioration Types on IRI and Rehabilitation. Transp. Res. Rec.

Anyala, M., Odoki, J.B., Baker, C.J., 2014. Hierarchical asphalt pavement deterioration model for climate impact studies. Int. J. Pavement Eng. 15, 251–266. https://doi.org/10.1080/10298436.2012.687105

Asadi, M., Nazarian, S., Mallick, R.B., Tirado, C., 2020. Computational Process for Quantifying the Impact of Flooding on Remaining Life of Flexible Pavement Structures. J. Transp. Eng. Part B Pavements 146, 04020060. https://doi.org/10.1061/JPEODX.0000219

Bubeck, P., Thieken, A.H., 2018. What helps people recover from floods? Insights from a survey among flood-affected residents in Germany. Reg. Environ. Change 18, 287–296. https://doi.org/10.1007/s10113-017-1200-y

Butt, A.A., Shahin, M.Y., Feighan, K.J., Carpenter, S.H., 1987. Pavement Performance Prediction Model Using the Markov Process. Transp. Res. Rec.

CDOT Online Transportation Information System [WWW Document], 2021. . Colo. Dep. Transp. URL https://dtdapps.coloradodot.info/otis

Chinowsky, P.S., Price, J.C., Neumann, J.E., 2013. Assessment of climate change adaptation costs for the U.S. road network. Glob. Environ. Change 23, 764–773. https://doi.org/10.1016/j.gloenvcha.2013.03.004

Chriestenson, C., Thilmany, D., 2020. Do factors contributing to appearance and success of conservation referenda in the West differ from those found in other regions of the United States? Ann. Reg. Sci. 65, 83–104. https://doi.org/10.1007/s00168-020-00975-7

Elshaer, M., Ghayoomi, M., Daniel, J.S., 2019. Impact of subsurface water on structural performance of inundated flexible pavements. Int. J. Pavement Eng. 20, 947–957. https://doi.org/10.1080/10298436.2017.1366767

First Street Foundation, 2020. The First National Flood Risk Assessment: Defining America's Growing Risk. First Street Foundation.

Gaspard, K., Martinez, M., Zhang, Z., Wu, Z., 2007. Impact of Hurricane Katrina on Roadways in the New Orleans Area (Technical Report No. 07–2TA). Louisiana Department of Transportation and Development - Louisiana Transportation Research Center.

Gaspard, K., Zhang, Z., Gautreau, G.P., Abufarsakh, M., Martinez, M., 2019. Impact of Inundation on Roadway Pavements: Case Study– LA 493 (Tech Report No. FHWA/LA.18/608), US Transportation Collection. Louisiana State University (Baton Rouge, La.). Department of Civil and Environmental Engineering, Louisiana. Department of Transportation and Development.

Geoff, G., 2011. Understanding floods: Questions & Answers. Queensland Government.

Gochis, D., Schumacher, R., Friedrich, K., Doesken, N., Kelsch, M., Sun, J., Ikeda, K., Lindsey, D., Wood, A., Dolan, B., Matrosov, S., Newman, A., Mahoney, K., Rutledge, S., Johnson, R., Kucera, P., Kennedy, P., Sempere-Torres, D., Steiner, M., Roberts, R., Wilson, J., Yu, W., Chandrasekar, V., Rasmussen, R., Anderson,

A., Brown, B., 2015. The Great Colorado Flood of September 2013. Bull. Am. Meteorol. Soc. 96, 1461–1487. https://doi.org/10.1175/BAMS-D-13-00241.1

Gulen, S., Woods, R., Weaver, J., Anderson, V.L., 1994. Correlation of Present Serviceability Ratings with International Roughness Index. Transp. Res. Rec.

Hamill, T.M., 2014. Performance of Operational Model Precipitation Forecast Guidance during the 2013 Colorado Front-Range Floods. Mon. Weather Rev. 142, 2609–2618. https://doi.org/10.1175/MWR-D-14-00007.1

Hashemi Tari, Y., Shahini Shamsabadi, S., Birken, R., Wang, M., 2015. Deterioration modeling for condition assessment of flexible pavements considering extreme weather events, in: Shull, P.J. (Ed.), . Presented at the SPIE Smart Structures and Materials + Nondestructive Evaluation and Health Monitoring, San Diego, California, United States, p. 943721. https://doi.org/10.1117/12.2084103

Helali, K., Robson, M., Nicholson, R., Bekheet, W., 2008. Importance of a Pavement Management System in Assessing Pavement Damage from Natural Disasters: A Case Study to Assess the Damage from Hurricanes Katrina and Rita in Jefferson Parish, Louisiana. Presented at the Seventh International Conference on Managing Pavement Assets Transportation Research Board Alberta Infrastructure and Transportation, Canada Federal Highway Administration.

Jackson, N.C., Puccinelli, J., 2006. Long-term Pavement Performance (LTPP) data analysis support: National Pooled Fund Study TPF-5(013). Effects of multiple freeze cycles and deep frost penetration on pavement performance and cost. US Department of Transportation, Federal Highway Administration, Research, Development, and Technology, Turner-Fairbank Highway Research Center, McLean, VA.

Kanti Sen, M., Dutta, S., Gandomi, A.H., Putcha, C., 2021. Case Study for Quantifying Flood Resilience of Interdependent Building–Roadway Infrastructure Systems. ASCE-ASME J. Risk Uncertain. Eng. Syst. Part Civ. Eng. 7, 04021005. https://doi.org/10.1061/AJRUA6.0001117

Karl, T.R., Meililllo, J.M., Peterson, T.C., 2009. Global Climate Change Impacts in the United States. Cambridge University Press, New York.

Keleman, M., Henry, S., Farrokhyar, A., Mero, B., Strome, G., Olson, S., 2008. Pavement Management Manual. Colorado Department of Transportation.

Khan, M.U., Mesbah, M., Ferreira, L., Williams, D.J., 2019. A case study on pavement performance due to extreme moisture intrusion at untreated layers. Int. J. Pavement Eng. 20, 1309–1322. https://doi.org/10.1080/10298436.2017.1408272

Khan, M.U., Mesbah, M., Ferreira, L., Williams, D.J., 2017a. Development of a post-flood road maintenance strategy: case study Queensland, Australia. Int. J. Pavement Eng. 18, 702–713. https://doi.org/10.1080/10298436.2015.1121781

Khan, M.U., Mesbah, M., Ferreira, L., Williams, D.J., 2017b. Estimating Pavement's Flood Resilience. J. Transp. Eng. Part B Pavements 143, 04017009. https://doi.org/10.1061/JPEODX.0000007

Khan, M.U., Mesbah, M., Ferreira, L., Williams, D.J., 2017c. Assessment of flood risk to performance of highway pavements. Proc. Inst. Civ. Eng. - Transp. 170, 363–372. https://doi.org/10.1680/jtran.15.00120

Khan, M.U., Mesbah, M., Ferreira, L., Williams, D.J., 2016. Preflood Road Maintenance Strategy for a Road Authority. J. Transp. Eng. 142, 04016068. https://doi.org/10.1061/(ASCE)TE.1943-5436.0000901

Khan, M.U., Mesbah, M., Ferreira, L., Williams, D.J., 2014. Developing a new road deterioration model incorporating flooding. Proc. Inst. Civ. Eng. - Transp. 167, 322–333. https://doi.org/10.1680/tran.13.00095

Lehmann, J., Coumou, D., Frieler, K., 2015. Increased record-breaking precipitation events under global warming. Clim. Change 132, 501–515. https://doi.org/10.1007/s10584-015-1434-y

Lu, D., Tighe, S., Xie, W.-C., 2018. Impact of flood hazards on pavement performance. Int. J. Pavement Eng. 21, 1–7. https://doi.org/10.1080/10298436.2018.1508844

Mallick, R.B., Tao, M., Daniel, J.S., Jacobs, J.M., Veeraragavan, A., 2017. Combined Model Framework for Asphalt Pavement Condition Determination After Flooding. Transp. Res. Rec. 2639, 64–72. https://doi.org/10.3141/2639-09

Martinez, M., Bakheet, R., Akib, S., 2021. Innovative Techniques in the Context of Actions for Flood Risk Management: A Review. Eng 2, 1–11. https://doi.org/10.3390/eng2010001

Mechanistic Empirical Pavement Design Guide, 2004. . U.S Department of Transportation - Federal Highway Administration.

Meyer, M., Flood, M., Keller, J., Lennon, J., McVoy, G., Dorney, C., Leonard, K., Hyman, R., Smith, J., 2014. Strategic Issues Facing Transportation, Volume 2: Climate Change, Extreme Weather Events, and the Highway System: Practitioner's Guide and Research Report. The National Academies Press, Washington, DC.

National Flood Hazard Layer (NFHL) Status [WWW Document], 2021. . Fed. Emerg. Manag. Agency. URL https://www.floodmaps.fema.gov/NFHL/status.shtml

Nazarian, S., Yuan, D., 2012. Variation in Moduli of Base and Subgrade with Moisture 570–577. https://doi.org/10.1061/40971(310)71

Neumann, J.E., Price, J., Chinowsky, P., Wright, L., Ludwig, L., Streeter, R., Jones, R., Smith, J.B., Perkins, W., Jantarasami, L., Martinich, J., 2015. Climate change risks to US infrastructure: impacts on roads, bridges, coastal development, and urban drainage. Clim. Change 131, 97–109. https://doi.org/10.1007/s10584-013-1037-4

NOAA's Weather and Climate Toolkit [WWW Document], 2021. . Natl. Ocean. Atmospheric Adm. URL https://www.ncdc.noaa.gov/wct/

Osorio-Lird, A., Chamorro, A., Videla, C., Tighe, S., Torres-Machi, C., 2017. Application of Markov chains and Monte Carlo simulations for developing pavement performance models for urban network management. Struct. Infrastruct. Eng.

Pérez-Acebo, H., Linares-Unamunzaga, A., Rojí, E., Gonzalo-Orden, H., 2020. IRI Performance Models for Flexible Pavements in Two-Lane Roads until First Maintenance and/or Rehabilitation Work. Coatings 10, 97. https://doi.org/10.3390/coatings10020097

Pérez-Acebo, H., Mindra, N., Railean, A., Rojí, E., 2019. Rigid pavement performance models by means of Markov Chains with half-year step time. Int. J. Pavement Eng. 20, 830–843. https://doi.org/10.1080/10298436.2017.1353390

Pulugurta, H., Shao, Q., Chou, Y.J., 2013. Pavement condition prediction using Markov process. J. Stat. Manag. Syst.

QGIS [WWW Document], 2021. . QGIS. URL https://qgis.org/en/site/

Qiao, Y., Santos, J., Stoner, A.M.K., Flinstch, G., 2020. Climate change impacts on asphalt road pavement construction and maintenance: An economic life cycle

assessment of adaptation measures in the State of Virginia, United States. J. Ind. Ecol. 24, 342–355. https://doi.org/10.1111/jiec.12936

Romanoschi, S., 2019. The Impact of Hurricane Harvey on Pavement Structures in the South East Texas and South West Louisian (No. Project No. 18PUTA02). Transportation Consortium of South-Central States (Tran-SET).

Saad, B., 2014. Analysis of excess water impact on the structural performance of flexible pavements. Int. J. Pavement Eng. 15, 409–426. https://doi.org/10.1080/10298436.2013.790546

Schweikert, A., Chinowsky, P., Espinet, X., Tarbert, M., 2014. Climate Change and Infrastructure Impacts: Comparing the Impact on Roads in ten Countries through 2100. Procedia Eng. 78, 306–316. https://doi.org/10.1016/j.proeng.2014.07.072

Sericola, B., 2013. Markov Chains: Theory and Applications. John Wiley & Sons.

Shamsabadi, S.S., Tari, Y.S.H., Birken, R., Wang, M., 2014. Deterioration Forecasting in Flexible Pavements Due to Floods and Snow Storms. Presented at the 7th European Workshop on Structural Health Monitoring, Nantes, France, p. 9.

Sultana, M., Chai, G., Chowdhury, S., Martin, T., 2016a. Rapid Deterioration of Pavements Due to Flooding Events in Australia 104–112. https://doi.org/10.1061/9780784480052.013

Sultana, M., Chai, G., Chowdhury, S., Martin, T., Anissimov, Y., Rahman, A., 2018a. Rutting and Roughness of Flood-Affected Pavements: Literature Review and Deterioration Models. J. Infrastruct. Syst. 24. https://doi.org/10.1061/(ASCE)IS.1943-555X.0000413

Sultana, M., Chai, G., Chowdhury, S., Martin, T., Anissimov, Y., Rahman, A., 2018b. Rutting and Roughness of Flood-Affected Pavements: Literature Review and Deterioration Models. J. Infrastruct. Syst. 24. https://doi.org/10.1061/(ASCE)IS.1943-555X.0000413

Sultana, M., Chai, G., Martin, T., Chowdhury, S., 2016b. Modeling the Postflood Short-Term Behavior of Flexible Pavements. J. Transp. Eng. 142, 04016042. https://doi.org/10.1061/(ASCE)TE.1943-5436.0000873

Sultana, M., Chai, G., Martin, T., Chowdhury, S., 2015. A Study on the Flood Affected Flexible Pavements in Australia 14.

Sultana, M., Chai, G., Martin, T., Chowdhury, S., 2014. A review of the structural performance of flooded pavements, in: A Review of the Structural Performance of Flooded Pavements. Presented at the ARRB Conference, 26th, 2014, Sydney, New South Wales, Australia.

Sultana, M., Chowdhury, S., Chai, G., Martin, T., 2016c. Modelling rapid deterioration of flooded pavements. Road Transp. Res. 25, 3–14.

Tabari, H., 2020. Climate change impact on flood and extreme precipitation increases with water availability. Sci. Rep. 10, 13768. https://doi.org/10.1038/s41598-020-70816-2

Texas Department of Transportation, T.D. of T., 2019. Asset Management, Extreme Weather, and Proxy Indicators Pilot Final Report. Texas Department of Transportation.

Thomas, O., Sobanjo, J., 2013. Comparison of Markov Chain and Semi-Markov Models for Crack Deterioration on Flexible Pavements. J. Infrastruct. Syst. 19, 186–195. https://doi.org/10.1061/(ASCE)IS.1943-555X.0000112

Torres-Machi, C., Chamorro, A., Yepes, V., Pellicer, E., 2014. Current models and practices of economic and environmental evaluation for sustainable network-level pavement management. Rev. Constr. 13, 49–56. https://doi.org/10.4067/S0718-915X2014000200006

Torres-Machi, C., Pellicer, E., Yepes, V., Chamorro, A., 2017. Towards a sustainable optimization of pavement maintenance programs under budgetary restrictions. J. Clean. Prod. 148, 90–102. https://doi.org/10.1016/j.jclepro.2017.01.100

Underwood, B.S., Guido, Z., Gudipudi, P., Feinberg, Y., 2017. Increased costs to US pavement infrastructure from future temperature rise. Nat. Clim. Change 7, 704–707. https://doi.org/10.1038/nclimate3390

Unterberger, C., 2018. How Flood Damages to Public Infrastructure Affect Municipal Budget Indicators. Econ. Disasters Clim. Change 2, 5–20. https://doi.org/10.1007/s41885-017-0015-0

US Department of Commerce, N., n.d. Flood Related Hazards [WWW Document]. URL https://www.weather.gov/safety/flood-hazards (accessed 6.8.21).

Veettil, P.C., Raghu, P.T., Ashok, A., 2021. Information quality, adoption of climate-smart varieties and their economic impact in flood-risk areas. Environ. Dev. Econ. 26, 45–68. https://doi.org/10.1017/S1355770X20000212

Vermont Agency of Transportation (VTrans), 2012. Adapting Vermont's Transportation Infrastructure to the Future Impacts of Climate Change, VTrans Climate Change Adaptation White Paper. Vermont Agency of Transportation, Montpelier, Vermont.

Wall, T., Meyer, M., 2013. Risk-Based Adaptation Frameworks for Climate Change Planning in the Transportation Sector. A Synthesis of Practice. https://doi.org/10.17226/22462

Wang, Y., Huang, Y., Rattanachot, W., Lau, K.K. (Woody), Suwansawas, S., 2015. Improvement of Pavement Design and Management for More Frequent Flooding Caused by Climate Change. Adv. Struct. Eng. 18, 487–496. https://doi.org/10.1260/1369-4332.18.4.487

Yamany, M.S., Abraham, D.M., Labi, S., 2021. Comparative Analysis of Markovian Methodologies for Modeling Infrastructure System Performance. J. Infrastruct. Syst. 27, 04021003. https://doi.org/10.1061/(ASCE)IS.1943-555X.0000604

Yang, J., Gunaratne, M., Lu, J.J., Dietrich, B., 2005. Use of Recurrent Markov Chains for Modeling the Crack Performance of Flexible Pavements. J. Transp. Eng. 131, 861–872. https://doi.org/10.1061/(ASCE)0733-947X(2005)131:11(861)

Yu-Shan, A., Shakiba, M., 2021. Flooded Pavement: Numerical Investigation of Saturation Effects on Asphalt Pavement Structures. J. Transp. Eng. Part B Pavements 147, 04021025. https://doi.org/10.1061/JPEODX.0000276

Zhang, Z., Wu, Z., Martinez, M., Gaspard, K., 2008. Pavement Structures Damage Caused by Hurricane Katrina Flooding. J. Geotech. Geoenvironmental Eng. 134, 633–643. https://doi.org/10.1061/(ASCE)1090-0241(2008)134:5(633)